Pattaradilokrat, S., Cheesman, S.J., Carter, R., 2008. Congenicity and genetic polymorphism in cloned lines derived from a single isolate of a rodent malaria parasite. Mol. Biochem. Parasitol. 157, 244–247.

Pattaradilokrat, S., Culleton, R.L., Cheesman, S.J., Carter, R., 2009. Gene encoding erythrocyte binding ligand linked to blood stage multiplication rate phenotype in *Plasmodium yoelii yoelii*. Proc. Natl. Acad. Sci. U.S.A. 106, 7161–7166.

Prasad, C.D., Prasad Singh, A., Chitnis, C.E., Sharma, A., 2003. A *Plasmodium yoelii yoelii* erythrocyte binding protein that uses Duffy binding-like domain for invasion: a rodent model for studying erythrocyte invasion. Mol. Biochem. Parasitol. 128, 101–105.

Pruenster, M., Rot, A., 2006. Throwing light on DARC. Biochem. Soc. Trans. 34, 1005–1008.

Reed, M.B., Caruana, S.R., Batchelor, A.H., Thompson, J.K., Crabb, B.S., Cowman, A.F., 2000. Targeted disruption of an erythrocyte binding antigen in *Plasmodium falciparum* is associated with a switch toward a sialic acid-independent pathway of invasion. Proc. Natl. Acad. Sci. U.S.A. 97, 7509–7514.

Reilly, H.B., Wang, H., Steuter, J.A., Marx, A.M., Ferdig, M.T., 2007. Quantitative dissection of clone-specific growth rates in cultured malaria parasites. Int. J. Parasitol. 37, 1599–1607.

Rodriguez, M., Lustigman, S., Montero, E., Oksov, Y., Lobo, C.A., 2008. PfRH5: a novel reticulocyte-binding family homolog of *Plasmodium falciparum* that binds to the erythrocyte, and an investigation of its receptor. PLoS One 3, e3300.

Rowe, J.A., Moulds, J.M., Newbold, C.I., Miller, L.H., 1997. *P. falciparum* rosetting mediated by a parasite-variant erythrocyte membrane protein and complement-receptor 1. Nature 388, 292–295.

Sali, A., Blundell, T.L., 1993. Comparative protein modelling by satisfaction of spatial restraints. J. Mol. Biol. 234, 779–815.

Sayle, R.A., Milner-White, E.J., 1995. RASMOL: biomolecular graphics for all. Trends Biochem. Sci. 20, 374.

Sim, B.K., Chitnis, C.E., Wasniowska, K., Hadley, T.J., Miller, L.H., 1994. Receptor and ligand domains for invasion of erythrocytes by *Plasmodium falciparum*. Science 264, 1941–1944.

Sim, B.K., Orlandi, P.A., Haynes, J.D., Klotz, F.W., Carter, J.M., Camus, D., Zegans, M.E., Chulay, J.D., 1990. Primary structure of the 175K *Plasmodium falciparum* erythrocyte binding antigen and identification of a peptide which elicits antibodies that inhibit malaria merozoite invasion. J. Cell Biol. 111, 1877–1884.

Stubbs, J., Simpson, K.M., Triglia, T., Plouffe, D., Tonkin, C.J., Duraisingh, M.T., Maier, A.G., Winzeler, E.A., Cowman, A.F., 2005. Molecular mechanism for switching of *P. falciparum* invasion pathways into human erythrocytes. Science 309, 1384–1387.

Swardson-Olver, C.J., Dawson, T.C., Burnett, R.C., Peiper, S.C., Maeda, N., Avery, A.C., 2002. *Plasmodium yoelii* uses the murine Duffy antigen receptor for chemokines as a receptor for normocyte invasion and an alternative receptor for reticulocyte invasion. Blood 99, 2677–2684.

Torii, M., Adams, J.H., Miller, L.H., Aikawa, M., 1989. Release of merozoite dense granules during erythrocyte invasion by *Plasmodium knowlesi*. Infect. Immun. 57, 3230–3233.

Tournamille, C., Colin, Y., Cartron, J.P., Le Van Kim, C., 1995. Disruption of a GATA motif in the Duffy gene promoter abolishes erythroid gene expression in Duffy-negative individuals. Nat. Genet. 10, 224–228.

Treeck, M., Struck, N.S., Haase, S., Langer, C., Herrmann, S., Healer, J., Cowman, A.F., Gilberger, T.W., 2006. A conserved region in the EBL proteins is implicated in microneme targeting of the malaria parasite *Plasmodium falciparum*. J. Biol. Chem. 281, 31995–32003.

Walliker, D., 1981. The genetics of virulence in *Plasmodium yoelii*. In: Cunning, E.U. (Ed.), Parasitological Topics, Special Publication No. 1, the Society of Protozoologists. Allen, Kansas, pp. 260–265.

Walliker, D., Sanderson, A., Yoeli, M., Hargreaves, B.J., 1976. A genetic investigation of virulence in a rodent malaria parasite. Parasitology 72, 183–194.

Wertheimer, S.P., Barnwell, J.W., 1989. *Plasmodium vivax* interaction with the human Duffy blood group glycoprotein: identification of a parasite receptor-like protein. Exp. Parasitol. 69, 340–350.

Withers-Martinez, C., Haire, L.F., Hackett, F., Walker, P.A., Howell, S.A., Smerdon, S.J., Dodson, G.G., Blackman, M.J., 2008. Malarial EBA-175 region VI crystallographic structure reveals a KIX-like binding interface. J. Mol. Biol. 375, 773–781.

Yeoh, S., O'Donnell, R.A., Koussis, K., Dluzewski, A.R., Ansell, K.H., Osborne, S.A., Hackett, F., Withers-Martinez, C., Mitchell, G.H., Bannister, L.H., Bryans, J.S., Kettleborough, C.A., Blackman, M.J., 2007. Subcellular discharge of a serine protease mediates release of invasive malaria parasites from host erythrocytes. Cell 131, 1072–1083.

Yoeli, M., Hargreaves, B., Carter, R., Walliker, D., 1975. Sudden increase in virulence in a strain of *Plasmodium berghei yoelii*. Ann. Trop. Med. Parasitol. 69, 173–178.

Zimmerman, P.A., Woolley, I., Masinde, G.L., Miller, S.M., McNamara, D.T., Hazlett, F., Mgone, C.S., Alpers, M.P., Genton, B., Boatin, B.A., Kazura, J.W., 1999. Emergence of FY*A(null) in a *Plasmodium vivax*-endemic region of Papua New Guinea. Proc. Natl. Acad. Sci. U.S.A. 96, 13973–13977.

Please cite this article in press as: Culleton, R., Kaneko, O., Erythrocyte binding ligands in malaria parasites: Intracellular trafficking and parasite virulence. Acta Trop. (2009), doi:10.1016/j.actatropica.2009.10.025

Chemistry and Physics of Lipids 160 (2009) 114–120

Contents lists available at ScienceDirect

Chemistry and Physics of Lipids

journal homepage: www.elsevier.com/locate/chemphyslip

Short communication

Different behavior of artemisinin and tetraoxane in the oxidative degradation of phospholipid

Naokazu Kumura[a], Hirotaka Furukawa[a], Arnold N. Onyango[b], Minoru Izumi[a], Shuhei Nakajima[a], Hideyuki Ito[c], Tsutomu Hatano[c], Hye-Sook Kim[c], Yusuke Wataya[c], Naomichi Baba[a,*]

[a] Graduate School of Natural Science and Technology, Okayama University, Okayama 700-8530, Japan
[b] Department of Food Science and Technology, Jomo Kenyatta University of Agriculture and Technology, P.O. Box 62000, Nairobi, Kenya
[c] Faculty of Pharmaceutical Science, Okayama University, Okayama 700-8530, Japan

ARTICLE INFO

Article history:
Received 4 September 2008
Received in revised form 27 April 2009
Accepted 28 April 2009
Available online 6 May 2009

Keywords:
Phospholipid
Artemisinin
Tetraoxane
Endoperoxide
Reactive oxygen species

ABSTRACT

The reaction of trioxane and tetraoxane endoperoxides with unsaturated phospholipid **1** in the presence of Fe(II) was investigated in the absence of oxygen by means of tandem ESI-MS analysis. The spectral analyses for the reaction mixtures showed that artemisinin **2** with a trioxane structure gave no peak except that for the remaining intact phospholipid **1** (*m/z* 758.9), indicating that there was no structural change to **1**. On other hand, the reaction mixture of **1** with tetraoxanes **3** and **4** afforded a number of new peaks (*m/z* 620–850) that were presumably assigned to oxidative degradation products originating from phospholipid **1**. Since this reaction was completely inhibited by the addition of a phenolic antioxidant, the process was considered to involve some free radical species. The newly discovered marked differences in reactivity between the trioxane and the tetraoxanes possibly reflects their different anti-malarial mechanisms, and this reactivity may contribute to the classification of a number of anti-malarial endoperoxides whose mode of action is based on phospholipid oxidation.

1. Introduction

Due to global warming, the growing risk of malaria infection has been increasingly recognized throughout the world. Developing resistance in malaria parasites to anti-malarial compounds is also a difficult problem and it has driven chemists to synthesize new anti-malarial medicines (Warhurst, 1999; Trape, 2001; Marquino et al., 2003; Winstanley et al., 2004). Information regarding the mechanism of anti-malarial activity is very important for the design of new compounds with higher activity and selectivity. Despite the many studies that have been published so far, the mechanism is still not well understood yet (Stocks et al., 2007). Artemisinin **2** which is isolated from the leaves of *Artemisia annua* has a sesquiterpene with trioxane endoperoxide structure and has high anti-malarial activity, and has been used in the effective therapy of malaria (Luo and Shen, 1987; Klayman, 1993) (Scheme 1). This highly oxygenated bicyclic endoperoxide structure was shown to be essential for anti-malarial activity (Klayman, 1985). Therefore, extensive studies have been devoted to the creation of novel anti-malarial compounds that have an endoperoxide structure such as that found in artemisinin. Some of these compounds have a tetraoxane structure instead of trioxane and show comparable activity with artemisinin against *Plasmodium falciparum* (Kim et al., 1999; Tokuyasu et al., 2001; Iskra et al., 2003; Terent'v et al., 2007). Running parallel with the synthetic approach, extensive studies have also been carried out on the anti-malarial mechanisms of artemisinin (O'Neill and Gary, 2004) and tetraoxane (Opsenica et al., 2006), and reactive radical species such as carbon and oxygen radicals (ROS) are considered to be involved in both cases. O'Neill and Gary (2004) described a mechanism by which the trioxane structure in artemisinin is subjected to heme-catalyzed homolytic cleavage affording oxygen radicals which are converted to carbon radicals (R•) in the decomposed structure of artemisinin. The carbon radicals then induce lipid peroxidation to afford hydroperoxides via abstraction of bis(allylic hydrogen) of the non-conjugated polyunsaturated fatty acyl carbon chain (Scheme 2). These hydroperoxides are well known to generate highly reactive oxygen radicals by the action of Fe(II) and ROS thus exerting oxidative stress on the malaria parasite (Meshnick et al., 1993; Posner and Meshnick, 2001; Creek et al., 2005; Opsenica et al., 2006). It is also well known that these ROS cause oxidative damage to enzymes, receptors, biological signal molecules and polyunsaturated lipids in cell membrane (Thannickal and Fanburg, 2000; Posner and Meshnick, 2001; Olliaro et al., 2001). Thus, proliferation and growth of the malaria parasite may be regulated through the oxidative degradation of the cell membrane lipid bilayer structure. Using EPR experiments, Opsenica et al. (2006) found that Fe(II)-induced scission of tetraoxane endperoxide afforded only an

* Corresponding author. Tel.: +81 86 251 8292; fax: +81 86 251 8388.
E-mail address: babanaom@cc.okayama-u.ac.jp (N. Baba).

0009-3084/$ – see front matter © 2009 Elsevier Ireland Ltd. All rights reserved.
doi:10.1016/j.chemphyslip.2009.04.005

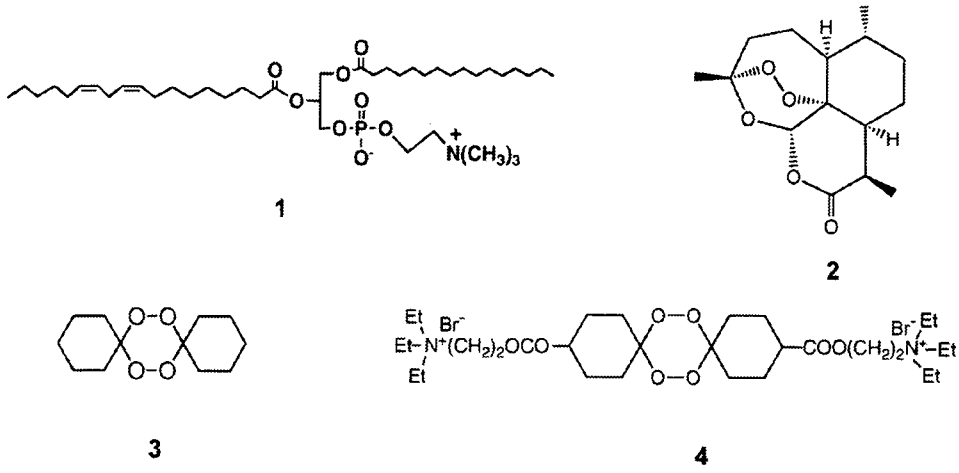

Scheme 1. The structure of 2-linoleoyl-1-palmitoyl-*sn*-phosphatidylcholine **1**, artemisinin **2**, tetraoxane **3**, and water-soluble tetraoxane derivative **4**.

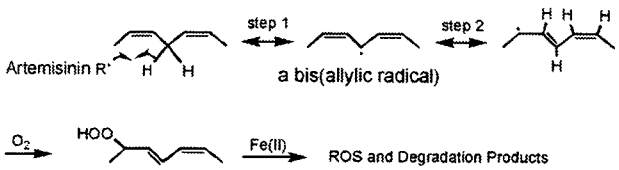

Scheme 2. Hypothetical mechanism of hydrogen abstraction from bis(allylic carbon) by the artemisinin radical followed by peroxidation and degradation affording ros and degradation products.

alkoxy radical RO•, and that this was responsible for the parasite's death. Our question is whether the oxygen or carbon radical produced from artemisinin can abstract the bis(allylic hydrogen atom) or not (step 1 in Scheme 2), since the hydrogen abstraction is the first step in olefine oxidation. The same questions arise naturally in the case of tetraoxane anti-malarial compounds. Thus, in the present study, artemisinin **2**, the less water-soluble tetraoxane **3** and the water-soluble **4** were examined to reveal whether they can induce oxidative degradation of olefines in 2-linoleoyl-1-palmitoyl-*sn*-glycerophosphocholine **1** (PC) as an in vitro model phospholipid (Scheme 1).

2. Experimental procedure

Phosphatidylcholine (PC) **1** (Baba et al., 1990) and the less water-soluble tetraoxane **3** (Berkessel et al., 2002) were prepared according to reported methods. Water-soluble tetraoxane **4** was prepared according to Scheme 3. The structure of all the intermediates and products were confirmed by ^{1}H NMR, ^{13}C NMR, IR and ESI-MS. NMR spectra were recorded using a 600 MHz Varian INOVA UNITY 600 spectrophotometer and the chemical shifts (δ) are expressed in ppm given relative to $CDCl_3$ (7.26 ppm for ^{1}H NMR, 77.00 ppm for ^{13}C NMR) or CD_3OD (3.30 ppm for ^{1}H NMR, 49.00 ppm for ^{13}C NMR). The IR spectra were recorded on a SHIMADZU IRPrestige-21. ESI-MS data were obtained using a Perkin–Elmer Model API-III by positive ion mode and direct infusion. High-resolution MS data were produced using Microsoft AutoSpec OA-Tof or Bruker micro TOF.

Caution: Although we did not encounter any difficulties while working with these tetraoxanes, we recommend routine precautions (avoidance of transition metal salts, broken glass and unnecessary heating) since organic peroxides are potentially hazardous.

2.1. Synthesis of bis(quaternary aminium salts) 4

2.1.1. Preparation of 7,8,15,16-tetraoxa-dispiro[5.2.5.2]hexadecane-3,12-dicarboxylic acid diethyl ester 6

Methyltrioxorhenium (VII) (MTO) (0.005 g, 0.02 mmol), 30% hydrogen peroxide (2.41 mL, 23.6 mmol) and sulfuric acid (0.634 mL, 11.9 mmol) were dissolved in hexafluoro-2-propanol (23 mL). Ethyl-4-oxocyclohexanecarboxylate **5** (2.00 g, 11.8 mmol) was added to the solution and stirred at room temperature (RT) for 5 min. Then excess manganese (IV) oxide was added and stirring was continued for an additional 15 min, followed by the addition of potassium carbonate (3.45 g, 25.0 mmol). The resulting mixture was filtered and the solvent evaporated under reduced pressure. The residue was chromatographed on silica gel (hexane/ethyl acetate = 7/3) affording tetraoxane **6** as a colorless powder (85% yield). IR ν_{max} (KBr): 2937, 2870, 1724, 1465, 1444, 1398, 1381, 1355, 1319, 1255, 1192, 1184, 1138, 1064, 1022, 985, 939, 920, 864, 808, 759, 678, 553 cm^{-1}; ^{1}H NMR ($CDCl_3$) δ: 1.24 (t, 6H, J = 7.3 Hz, $-COOCH_2CH_3 \times 2$), 1.52 (br, 2H, cyclohexyl protons), 1.82 (br, 12H, cyclohexyl protons), 2.39 (m, 2H, cyclohexyl protons), 2.87 (br, 2H, cyclohexyl protons), 4.12 (q, 4H, J = 7.3 Hz, $-COOCH_2CH_3 \times 2$); ^{13}C NMR ($CDCl_3$) δ: 14.17 ($-COOCH_2CH_3$), 23.72 (br), 24.59 (br), 28.01 (br), 30.27 (br), 41.56 (>CCOO–), 60.42 ($-COOCH_2CH_3$), 107.50 (>C(–O–O–)$_2$), 174.51 (–COOEt); ESI-MS $[M+NH_4]^+$ m/z 390.18. HRMS $[M+Na]^+$ m/z 395.1675. Calcd. for $[C_{18}H_{28}O_8+Na]^+$, m/z 395.1682.

2.1.2. Preparation of 7,8,15,16-tetraoxa-dispiro[5.2.5.2]hexadecane-3,12-dicarboxylic acid 7

Tetraoxane **6** (0.20 g, 0.59 mmol) was dissolved in a mixture of 73% aqueous methanol (10.4 mL). Sodium hydroxide (0.40 g, 10 mmol) was added to the solution and stirred at RT for 6 h. And the resulting mixture was then acidified to pH 3–4 with 1 M hydrochloric acid, followed by extraction with a mixture of chloroform/methanol (2:1, 5 × 30 mL). The combined organic layer was washed with brine (2 × 50 mL), dried over anhydrous sodium sulfate and concentrated *in vacuo* giving the desired compound **7** as a colorless powder (quant.). IR ν_{max} (KBr): 2943, 2872, 1691, 1463, 1423, 1342, 1319, 1220, 1136, 1066, 941, 914, 682, 555 cm^{-1}; ^{1}H NMR (CD_3OD) δ: 1.54 (br, 2H, cyclohexyl protons), 1.84 (br, 12H, cyclohexyl protons), 2.40 (m, 2H, cyclohexyl protons), 2.85 (br, 2H, cyclohexyl protons). ^{13}C NMR (CD_3OD) δ: 25.08 (br), 25.94

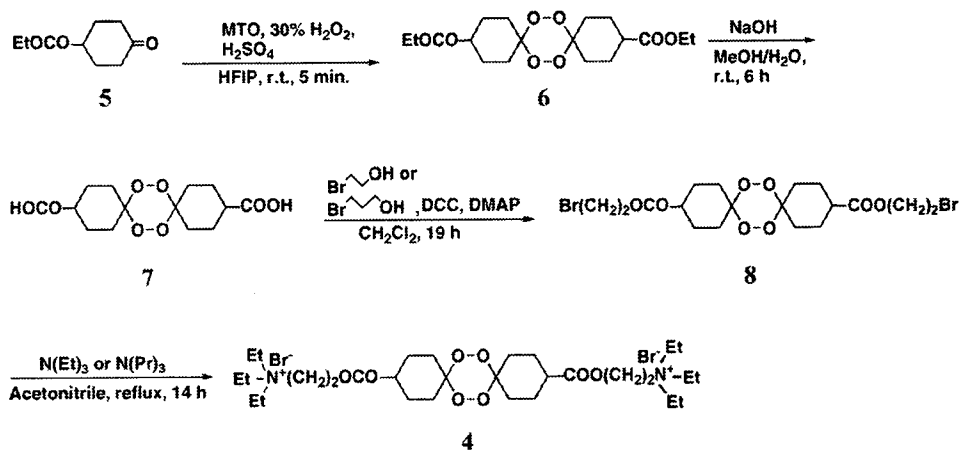

Scheme 3. Synthesis of water-soluble tetraoxane with bis(quaternaryammonium salt) structure.

(br), 29.12 (br), 31.29 (br), 42.55 (>CCOO–), 108.63 (>C(–O–O–)$_2$), 210.55 (–COOH). ESI-MS $[M+NH_4]^+$ *m/z* 334.10. HRMS $[M+Na]^+$ *m/z* 339.1056. Calcd. for $[C_{14}H_{20}O_8+Na]^+$, *m/z* 339.1054.

2.1.3. Preparation of 7,8,15,16-tetraoxa-dispiro[5.2.5.2]hexadecane-3,12-dicarboxylic acid bis(2-bromoethyl) ester ***8***

Tetraoxane **7** (0.38 g, 1.19 mmol), 2-bromoethanol (0.21 mL, 2.88 mmol), and 4-dimethylaminopyridine (0.24 g, 1.92 mmol) were dissolved in dichloromethane (20 mL). A solution of DCC (0.59 g, 2.88 mmol) in dichloromethane (5 mL) was added, and the reaction mixture was stirred at RT for 19 h in an atmosphere of nitrogen. The reaction mixture was filtered and the solvent was evaporated off under reduced pressure. Chromatography of the residue on silica gel (hexane/ethyl acetate = 3:1) afforded the tetraoxane ester **8** as a colorless powder (81% yield). IR ν_{max} (KBr): 2951, 2872, 1724, 1394, 1361, 1328, 1274, 1197, 1182, 1141, 1002, 974, 927, 657, 567 cm^{-1}; ^1H NMR ($CDCl_3$) δ: 1.49 (br, 2H, cyclohexyl protons), 1.75 (br, 12H, cyclohexyl protons), 2.42 (m, 2H, cyclohexyl protons), 2.80 (br, 2H, cyclohexyl protons), 3.46 (q, 4H, J = 5.9 Hz, $-COOCH_2CH_2Br \times 2$), 4.33 (t, 4H, J = 5.9 Hz, $-COOCH_2CH_2Br \times 2$). ^{13}C NMR ($CDCl_3$) δ: 23.48 (br), 24.39 (br), 27.76 (br), 28.80 ($-COOCH_2CH_2Br$), 29.98 (br), 41.10 (>CCOO–), 63.52 ($-COOCH_2CH_2Br$), 107.23 (>C(–O–O–)$_2$), 173.76 ($-COOCH_2CH_2Br$). ESI-MS $[M+NH_4]^+$ *m/z* 547.80. HRMS $[M+Na]^+$ *m/z* 552.9888. Calcd. for $[C_{18}H_{26}Br_2O_8+Na]^+$, *m/z* 552.9872.

2.1.4. Preparation of bis ester of triethyl-2-hydroxyethyl ammonium bromide with 7,8,15, 16-tetraoxa-dispiro[5.2.5.2]hexadecane-3,12-dicarboxylic acid ***4***

The tetraoxane bromo ester **8** (0.55 g, 1.03 mmol) and distilled triethylamine (10 mL, 7.2 mmol) were dissolved in acetonitrile (20 mL) and refluxed for 14 h. The solvent was evaporated under reduced pressure, and the residue was washed with a mixture of ether and acetone or ether and ethanol. Crystallization of the residue from a mixture of ethanol and diethyl ether gave the desired bis(quaternary ammonium salts) **4** as a colorless powder (28% yield). IR ν_{max} (KBr): 2924, 2854, 1741, 1456, 1400, 1321, 1257, 1224, 1184, 1172, 1136, 1085, 1060, 999, 939, 786, 669, 555 cm^{-1}; ^1H NMR (CD_3OD) δ: 1.33 (t, 18H, J = 7.3 Hz, $-N(CH_2CH_3)_3 \times 2$), 1.59 (br, 2H, cyclohexyl protons), 1.74 (br, 8H, cyclohexyl protons), 1.91 (br, 2H, cyclohexyl protons), 1.96 (br, 2H, cyclohexyl protons), 2.57 (m, 2H, cyclohexyl protons), 2.92 (br, 2H, cyclohexyl protons), 3.42 (q, 12H, J = 7.3 Hz, $-N(CH_2CH_3)_3 \times 2$), 3.63 (t, 4H, J = 4.9 Hz, $-COOCH_2CH_2NEt_3 \times 2$), 4.48 (t, 4H, J = 4.9 Hz, $-COOCH_2CH_2NEt_3 \times 2$). ^{13}C NMR (CD_3OD) δ: 7.74 ($-N(CH_2CH_3)_3$), 25.04 (br), 25.87 (br), 28.99 (br), 31.17 (br), 42.55 (>CCOO–), 54.65 ($-N(CH_2CH_3)_3$), 56.42 ($-COOCH_2CH_2NEt_3$), 58.47 ($-COOCH_2CH_2NEt_3$), 108.56 (>C(–O–O–)$_2$), 175.26 ($-COOCH_2CH_2NEt_3$). ESI-MS $[M-2Br]^{2+}$ *m/z* 286.20. HRMS $[M-2Br]^{2+}$ *m/z* 286.2023. Calcd. for $[C_{15}H_{28}NO_4]^{2+}$, *m/z* 286.2013.

2.2. Procedure for the reaction of PC ***1*** *with the endoperoxides,* ***2****,* ***3*** *and* ***4***

According to the methods reported by Creek et al. (2005) and Spickett et al. (1998), the following experiment was conducted with some modifications. A degassed aqueous solution of iron(II) sulfate (2.5 mL, 180 μmol) and that of endoperoxide in ethanol or water (2.0 mL, 50 μmol) were added to a solution of PC **1** in ethanol or water (0.5 mL, 25 μmol). After stirring at 37 °C for 24 h under a nitrogen or oxygen atmosphere, the solution was quenched with 50% aqueous phytic acid solution (0.17 mL, 180 μmol), and a trace of BHT was added to prevent further radical-induced degradation. The reaction mixture was filtered and the filtrate was then extracted using the Bligh–Dyer method (Bligh and Dyer, 1959) with a mixture of $CHCl_3/CH_3OH$ (1:2, 6.0 mL) and dried over anhydrous magnesium sulfate. After filtration, the filtrate was analyzed by tandem ESI-MS in precursor ion scan mode using *m/z* 184 as a product ion of the choline phosphate moiety (Khaselev and Purphy, 2000).

3. Result and discussion

As a preliminary experiment, the time course of the decrease in phospholipid **1** was traced from 0 to 27 h. The % intensity of the remaining intact **1** (*m/z* 758.8) in the ESI-MS spectrum of the total intensity of peaks in the same spectrum was calculated and plotted against the reaction time (Fig. 1). As shown in this figure, during the first hour, the decrease in **1** was very rapid, and after 10 h, the rate was slow. From this result, the reaction time was fixed to 24 h for all the experiments. The dose-dependence of reagents was also measured by changing the ratio of **1** to tetraoxane **3** from 10:1 to 1:2. Since the graphical expression of data appeared to be ambiguous, the data are shown as figures for each of the reaction mixtures. The reaction was conducted at ratios (**1**:tetraoxane) of 10:1, 2:1, 1:1 and 1:2, respectively, for 24 h, and the ESI-MS spectra of the each reaction mixture is given in Fig. 2. The results indicated that, at 10:1 (A in Fig. 2) and 2:1 (B), most of **1** (*m/z* 758.8) remained intact, and at 1:1 (C), a significant decrease in **1** was observed. Since the

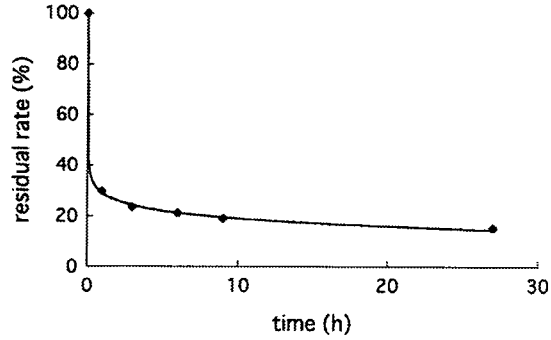

Fig. 1. Time-course of the reaction of tetraoxane **3** with phosphatidylcholine **1**. The reaction was conducted at 37 C. The data were obtained from the % relative intensity of unreacted **1** in the reaction mixture plotted against the sum of the intensity of each of the peaks in the ESI-MS spectrum.

reaction was remarkable (D) at 2:1, we fixed the ratio at 2:1 for all the experiments.

All the results from the degradation experiments obtained by ESI-MS are shown in Table 1. As a control experiment, the linoleic acid moiety in PC **1** was oxidized by the Fenton reaction using $FeSO_4$ in an atmosphere of oxygen, and the ESI-MS spectrum of this reaction mixture is shown in Fig. 3A in which the signal for the intact PC **1** at *m/z* 758.7 has completely disappeared and has been replaced by some new signals at *m/z* levels lower than 758.7. This indicated that the olefinic structure of PC **1** had been subjected to oxidative degradation by the Fenton system affording PC degradation products with lower molecular weights as expected from the lipid peroxidation process. On the other hand, as Fig. 3B shows, in the N_2 atmosphere, the degradation level was much lower, strongly indicating that molecular oxygen is involved in the oxidation process. Thus, the presence of Fe(II)-catalyzed auto-oxidation products of PC **1** was confirmed by ESI-MS.

First, to reveal whether or not artemisinin endoperoxide is involved in the lipid oxidation, we conducted a similar experiment in an O_2 or N_2 atmosphere. As shown in Fig. 3C, the ESI-MS spectrum for the former in the presence of O_2 was similar to Fig. 3A. On the other hand, in the absence of O_2, only a signal for intact PC **1** was observed at *m/z* 758.7 (Fig. 3D). These results convincingly demonstrated for the first time that artemisinin itself is not responsible for the oxidation of PC **1** even in the presence of Fe(II). Since the color of the reaction mixture changed from colorless to brown, Fe(II) was found to be converted to Fe(III) instantly after the addition of artemisinin. Also, ^1H NMR spectrum of the reaction mixture showed that the structure of artemisinin had decomposed. On the other hand, proton signals for the conjugated diene system (Scheme 2) in the NMR spectrum of PC **1** were not observed between 5.5 and 7.0 ppm except for a multiplet signal at 5.4 ppm which represented the four non-conjugated olefin protons in linoleic acid. This unambiguously indicated that during the reaction, no hydrogen radical was abstracted from the bis(allylic carbon) between the two olefinic structures of the linoleic acyl group, since as soon as the bis(allylic carbon) radical was formed it underwent 1,3-migration affording a more stable conjugated diene system and the four proton signals appeared at 5.5–7.0 ppm as multiplets (step 2 in Scheme 2). Therefore, even though some radical species were produced from artemisinin during the reaction, they did not appear to be able to abstract hydrogen radicals from the bis(allylic carbon). We conducted the same experiment using tetraoxane **3** in the presence of Fe(II) and absence of O_2. The ESI-MS spectrum of the reaction mixture is shown in Fig. 3E. This spectrum is similar to that shown in Fig. 3A for the Fe(II)-catalyzed oxidation of PC **1** under O_2 except for two peaks at *m/z* 622.9 and 683.8 that were not found in the spectrum shown in Fig. 3A, and the spectrum in Fig. 3E is missing the peak at *m/z* 652.8 which is illustrated in Fig. 3A. When an antioxidant butylated hydroxytoluene (BHT) was added to the reaction mixture, all the peaks except for *m/z* 759.0 of PC **1** disappeared (Fig. 3F), indicating that the PC degradation was completely inhibited by the antioxidant. Thus, even in the absence of O_2, the tetraoxane **3** oxidatively decomposed PC in the presence of Fe(II) and peroxidation appears to be the definitive radical pathway through which this process takes place as demonstrated by the inhibition with the antioxidant (Fig. 3F). This result was in marked contrast to that with artemisinin. Because of the low water-

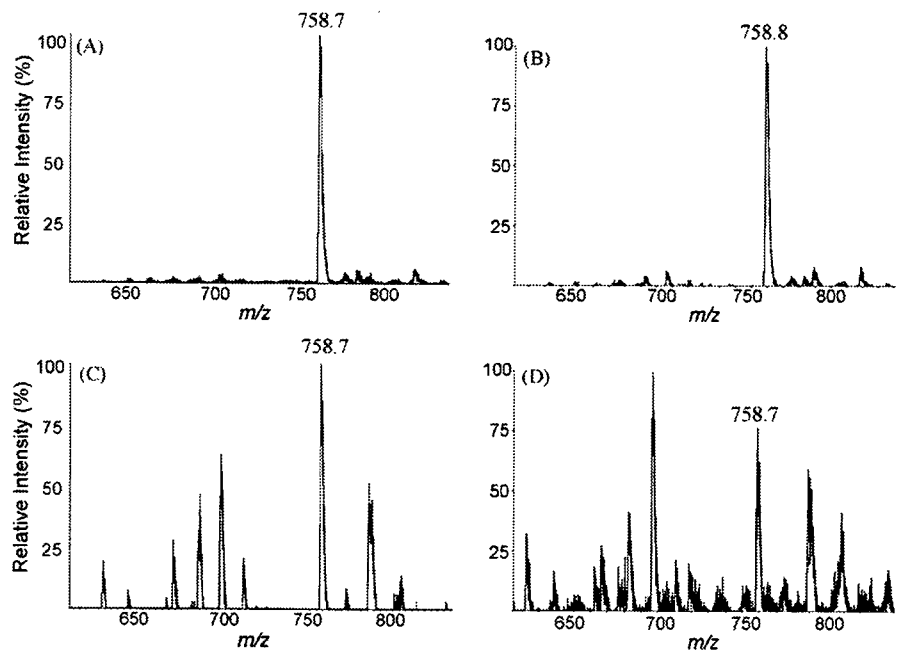

Fig. 2. Dose-dependence in the reaction of tetraoxane **3** with phosphatidylcholine **1** (*m/z* 758.7). The reaction was conducted at 37 °C for 24 h. (A) Molar ratio of **1**/**3** = 10:1, (B) **1**/**3** = 2:1, (C) **1**/**3** = 1:1 and (D) **1**/**3** = 1:2.

Table 1
ESI-MS data obtained from the oxidative degradation of PC **1** by O_2, artemisinin **2**, tetraoxane **3** and water-soluble tetraoxane **4**.

Entry	Reagent	Observed *m/z*								Degradation
1[a]	PC + Fe in O_2	624.8	638.5	652.8	666.5	680.6	696.4			Yes
2[a]	PC + Fe in N_2	758.9								Much less
3[a]	PC + Fe + **2** in O_2	624.8	638.6	652.8	666.6	680.7	696.8	756.9		Yes
4[a]	PC + Fe + **2** in N_2	758.7								No
5[a]	PC + Fe + **3** in N_2	622.9	638.6	666.7	680.7	683.8	696.8	758.7	788.9	Yes
6[a]	PC + Fe + **3** + BHT in N_2	759.0								No
7[b]	PC + Fe + **4** in N_2	622.6	638.7	666.8	680.6	683.1	696.8	758.8	788.9	Yes
8[b]	PC + Fe + **4** + BHT in N_2	758.9								No
9[b]	PC + Fe + **4**in N_2 622.8	638.7	666.8	680.6	683.6	696.9	758.9	788.8	808.8	Yes
10[b]	PC + Fe + **3** + BHT in N_2	758.9								No

[a] Experiments were performed in 50% aq. ethanol.
[b] Experiments were performed in distilled water.

solubility of the tetraoxane **3** and high water-solubility of Fe(II), 50% EtOH was used as a solvent to obtain the nearly homogeneous solution. This solvent system is, however, not always suitable for the total completion of the intermolecular interaction between the tetraoxane and the PC **1**. To obtain a completely aqueous solution in which all the reactants are completely dissolved, we used a water soluble conjugate of tetraoxane with bis(quaternary ammonium salts) **4** that was newly synthesized in the present study. Degassed distilled water was used here instead of 50% EtOH. Fig. 4A shows the ESI-MS spectrum of the mixture resulting from the reaction of **4** with PC **1** in 50% EtOH. When we compared this spectrum with that shown in Fig. 3E for **3** in 50% EtOH, peaks with the same *m/z* were observed and are listed in Table 1 (entries 7 and 8). The intensity of each peak in Fig. 4A was, however, considerably different from those observed in Fig. 3E. Fig. 4B shows the ESI-MS spectrum of the mixture resulting from the reaction of **4** with PC **1** in degassed water instead of 50% EtOH. In this case, since sonic treatment was used to solubilize PC **1**, the phospholipid molecules should exist as vesicles (Spickett et al., 1998). Although the spectrum was similar to that shown in Fig. 4A, four peaks at *m/z* 758.9 (unreacted PC **1**),

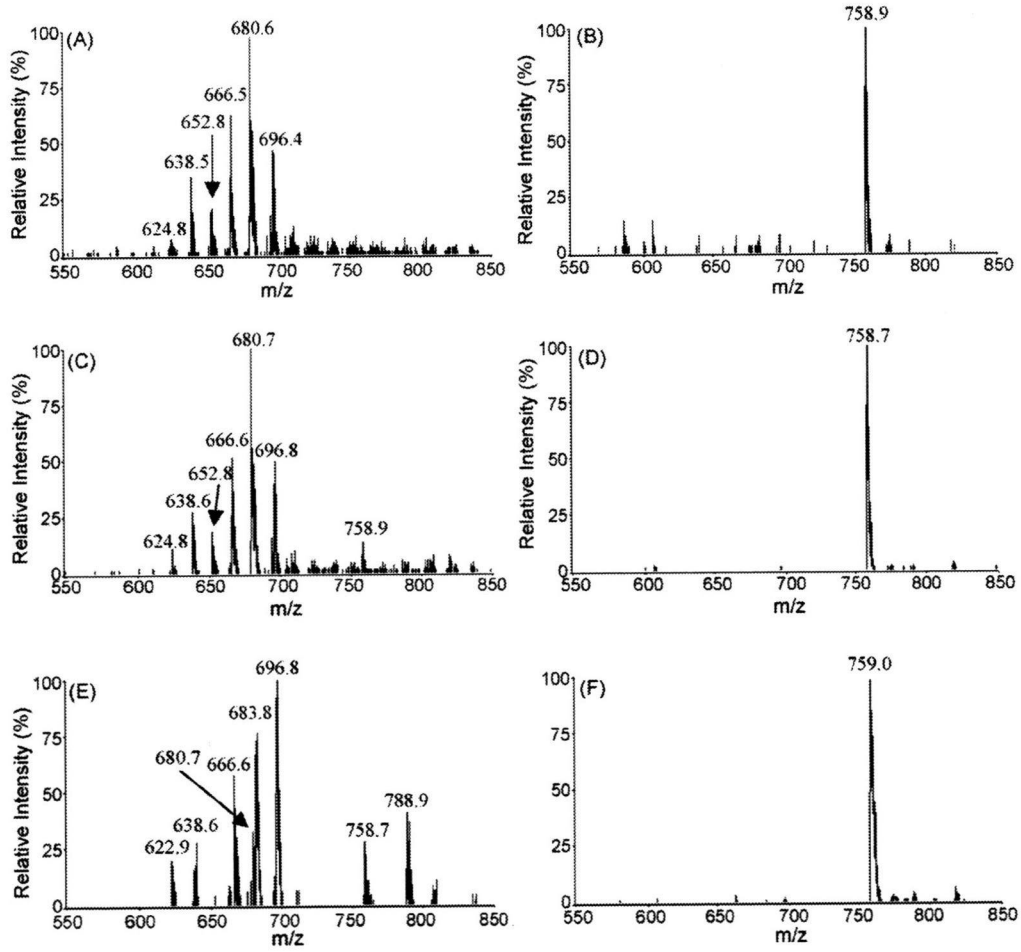

Fig. 3. ESI-MS Spectra of the product mixture from the reaction of 2-linoleoyl-1-palmitoyl-*sn*-glycero-phosphatidylcholine (PC **1**) and Fe(II) in 50% aq. ethanol. (A) In an O_2 atmosphere, (B) in a N_2 atmosphere, (C) with artemisinin in an O_2 atmosphere, (D) with artemisinin **2** in a N_2 atmosphere, (E) with tetraoxane **3** in a N_2 atmosphere and (F) with tetraoxane **3** in the presence of butylated hydroxytoluene (BHT) in a N_2 atmosphere.

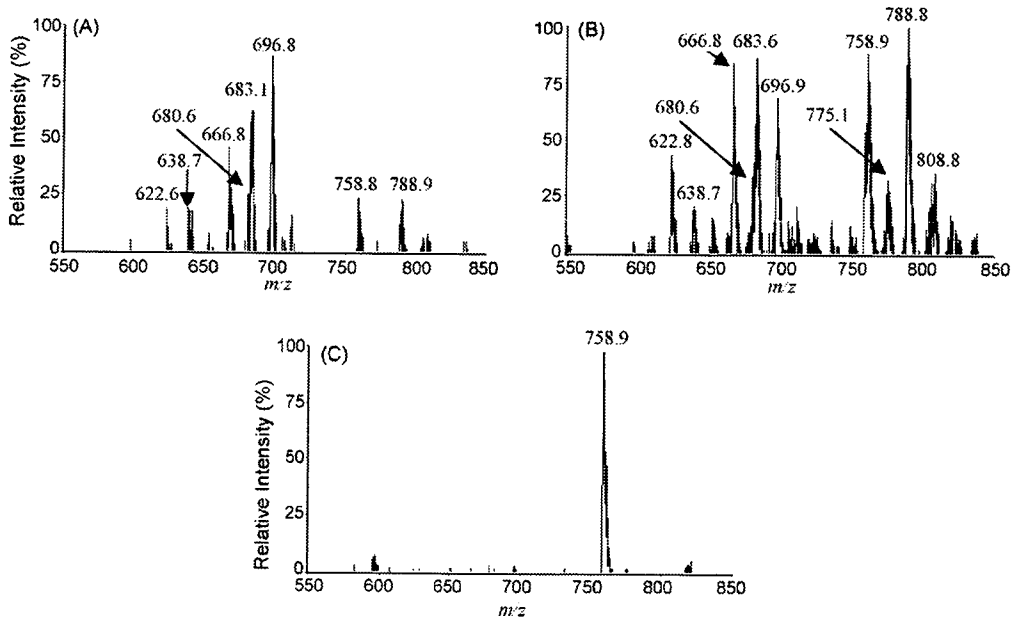

Fig. 4. ESI-MS spectra of the product mixture from the reaction of 2-linoleoyl-1-palmitoyl-*sn*-glycero-phosphatidylcholine (PC **1**) and Fe(II). (A) water-soluble tetraoxane **4** in 50% aq. ethanol and under a N_2 atmosphere, (B) water-soluble tetraoxane **4** in water and a N_2 atmosphere and (C) water-soluble tetraoxane **4** in water and a N_2 atmosphere in the presence of BHT.

775.1, 788.8 and 808.8 were significantly more intense. Thus, the water soluble endoperoxide **4** also behaved in a similar manner to **3** in the oxidation of PC **1** in both 50% EtOH and water. Here, the oxidative degradation of PC **1** with **4** in water was also completely inhibited by an antioxidant BHT (Fig. 4C). Finally, the presumed chemical structures for some of the degradation products are given in Scheme 4. They were deduced from the value of *m/z* according to the oxidative cleavage mechanisms reported to date (Kappus, 1985; Spiteller, 1998; Reis et al., 2004).

Artemisinin and tetraoxanes contain unstable bridged peroxide structures and are known to be very sensitive to transition metals such as Fe(II) and Cu(I) affording radical species. This is the first report of the induced oxidative cleavage of the polyunsaturated phospholipid by tetraoxane endoperoxides even in the absence of O_2 and prevention of this cleavage by a phenolic antioxidant. In contrast, artemisinin which contains the trioxane endoperoxide structure did not cause such a cleavage. Although a number of hypotheses for anti-malarial mechanisms have been reported to date, a general mechanism has not been established as yet. In the case of artemisinin, it has been claimed that carbon radicals from artemisinin interact with heme preventing its polymerization which is important in the growth and proliferation of malaria parasites. Another hypothesis suggests that as artemisinin is structurally different to tetraoxanes, it causes the destruction

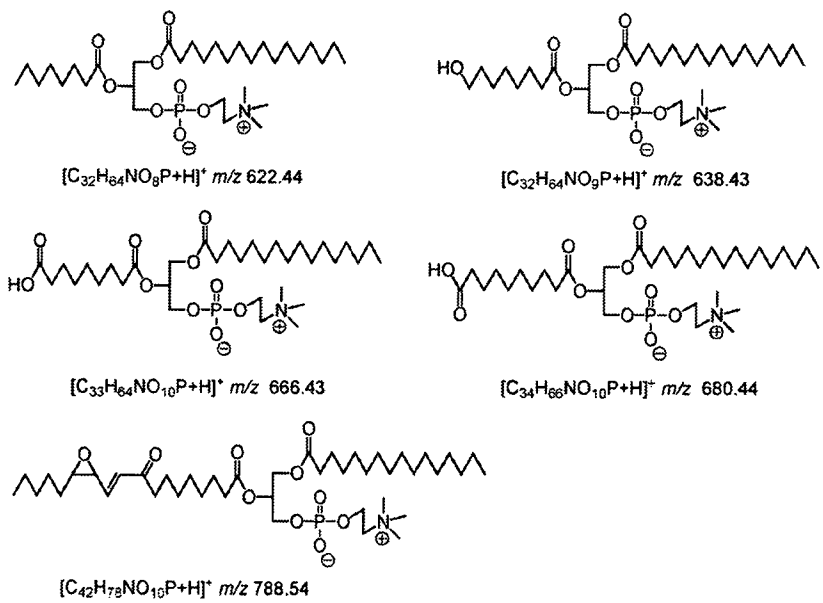

Scheme 4. The presumed structure of the degradation products from PC **1**.

of the malaria parasite cells to afford carbon radicals, which may induce oxidation of polyunsaturated phospholipids thus interfering with the normal constitution of the cell membranes of the malaria parasites. Based on our new observations in the present study, such a lipid oxidation may not occur with carbon radicals formed from artemisinin. Therefore, in the case of artemisinin, lipid oxidation may not be involved in the anti-malarial mechanism.

Although both the endoperoxides are highly active against the malaria parasite, their modes of actions are different. It has been reported that artemisinin inhibits a broad spectrum of ring and schizont stages of malaria parasites *in vitro* (Skinner et al., 1996) and it causes recrudescence of the parasites in malarial patients. In contrast, tetraoxanes including our compounds (Tsuchiya et al., 1999) specifically and completely inhibit the trophozoite stage *in vitro*. Therefore, if this stage is blocked by tetraoxanes, malaria parasites can no longer grow and proliferate. The structural difference between artemisinin and tetraoxane endoperoxides might be responsible for the different features of the anti-malarial action described above and also for the difference in reactivity during the decomposition of unsaturated phospholipid **1** described in the present paper. Therefore, if a reliable correlation is discovered in the future between the structures of endoperoxides, the anti-malarial mechanism, and their contribution to the decomposition of unsaturated phospholipid, this information will be of great value in the design of new anti-malarial compounds. It might also be expected to contribute to the classification of a diverse array of anti-malarial endoperoxides based on the reaction with polyunsaturated phospholipid.

Acknowledgments

We would like to thank Prof. Kenji Uneyama at Okayama University for his valuable advice with regard to the present study. We gratefully acknowledge the Central Glass Co. Ltd. for the gift of HFIP. Also, we would like to thank the laboratory of SC-NMR and the laboratory of API III mass spectrometry in Okayama University, Japan.

References

Baba, N., Yoneda, K., Tahara, S., Iwasa, J., Kaneko, T., Matsuo, M., 1990. A regioselective, stereoselective synthesis of a diacylglycerophosphocholine hydroperoxide by use of lipoxygenase and lipase. J. Chem. Soc. Chem. Commun. 18, 1281–1282.

Berkessel, A., Andreae, M.R.M., Schmickler, H., Lex, J., 2002. Baeyer-Villiger oxidations with hydrogenperoxide in fluorinated alcohols: lactone formatin by a nonclassical mechanism. Angew. Chem. Int. Ed. 41, 4481–4484.

Bligh, E.G., Dyer, W.J., 1959. A rapid method of total lipid extraction and purification. Can. J. Biochem. Physiol. 37, 911–917.

Creek, D.J., Chiu, F.C.K., Prankerd, R.J., Charman, S.A., Charman, W.N., 2005. Kinetics of iron-mediated artemisinin degradation: effect of solvent composition and iron salt. J. Pharm. Sci. 94, 1820–1829.

Iskra, J., Bonnet-Delpon, D., Begue, J.-P., 2003. One-pot synthesis of non-asymmetric tetraoxanes with H_2O_2, MTO, fluorous alcohol system. Tetrahedron Lett. 44, 6309–6312.

Kappus, H., 1985. Lipid peroxidation: mechanisms, analysis, enzymology and biological relevance. In: Sies, H. (Ed.), Oxidative Stress. Academic Press, London, pp. 273–310.

Khaselev, N., Purphy, R.C., 2000. Structural characterization of oxidized phospholipid products derived from arachidonate-containing plasmenyl glycerophosphocholine. J. Lipid Res. 41, 564–572.

Kim, H.-S., Shibata, Y., Wataya, U., Tsuchiya, K., Masuyama, A., Nojima, M., 1999. Synthesis and antimalarial activity of cyclic peroxides 1,2,4,5,7-pentoxocanes and 1,2,4,5-tetraoxanes. J. Med. Chem. 42, 2604–2606.

Klayman, D.L., 1985. Qinghaosu (artemisinin) – an antimalarial drug from China. Science 228, 1049–1055.

Klayman, D.L., 1993. *Artemisia-annua* – from weed to respectable antimalarial plant. ACS Symp. Ser. (USA) 534, 242–255.

Luo, X.D., Shen, C.C., 1987. The chemistry, pharmacology, and clinical applications of qinghaosu (artemisinin) and its derivatives. Med. Res. Rev. 7, 29–52.

Marquino, W., Huilca, M., Calampa, C., Falconi, E., Cavezas, C., 2003. Efficacy of mefloquine and a mefloquine-artesunate combination therapy for the treatment of uncomplicated *Plasmodium falciparum* malaria in the Amazon basin of Peru. Am. J. Trop. Med. Hyg. 68, 608–612.

Meshnick, S.R., Yang, Y.-Z., Lima, V., Kuypers, F., Klamchonwongpaisan, S., Yuthavong, Y., 1993. Iron-dependent free radical generation from the antimalarial agent artemisinin (Qinghaosu). Antimicrob. Agents Chemother. 37, 1108–1114.

Olliaro, P.L., Haynes, R.K., Meybuer, B., Yuthavong, Y., 2001. Possible modes of action of the artemisinin-type compounds. Trends Parasitol. 17, 122–126.

O'Neill, P.M., Gary, H.P., 2004. A medicinal chemistry perspective on artemisinin and related endoperoxides. J. Med. Chem. 47, 2945–2964.

Opsenica, I., Terzic, N., Opsenica, D., Angelovski, G., Lehnig, M., Eilbracht, P., Tinant, B., Juranic, Z., Smithy, K.S., Yang, Y.S., Diaz, D.S., Smith, P.L., Milhous, W.K., Dokovic, D., Solaja, B.A., 2006. A tetraoxane antimalarials and their reaction with Fe(II). J. Med. Chem. 49, 3790–3799.

Posner, G.H., Meshnick, S.R., 2001. Radical mechanism of action of the artemisinin-type compounds. Trends Parasitol. 17, 266–267.

Reis, A., Domingues, P., Ferrer-Correia, A.J.V., Domingues, M.R.M., 2004. Fragmentation study of short-chain products derived from oxidation of diacylphosphatidylcholines by electrospray tandem mass spectrometry: identification of novel short-chain products. Rapid Commun. Mass Spect. 18, 2849–2858.

Skinner, T.S., Manning, L.S., Johnston, W.A., Davis, T.M., 1996. In vitro stage-specific sensitivity of *Plasmodium falciparum* to quinine and artemisinin drugs. Int. J. Parasitol. 26, 519–525.

Spickett, C.M., Pitt, A.R., Brown, A.J., 1998. Direct observation of lipid hydroperoxides in phospholipid vesicles by electrospray mass spectrometry. Free Radic. Biol. Med. 25, 613–620.

Spiteller, G., 1998. Linoleic acid peroxidation—the dominant lipid peroxidation process in low density lipoprotein—and its relationship to chronic diseases. Chem. Phys. Lip. 95, 105–162.

Stocks, P.A., Bray, P.G., Barton, V.E., Al-Hela, M., Jones, M., Araujo, N.C., Gibbons, P., Stephen, A.W., Hughes, R.H., Biagini, G.A., Davies, J., Amewu, R., Mercer, A.E., Ellis, G., O'Neill, P.M., 2007. Evidence for a common non-heme chelatable-iron-dependent activation mechanism for semisynthetic and synthetic endoperoxide antimalarial drugs. Angew. Chem. 119, 6394–6399.

Terent'v, A.O., Kutkin, A.V., Starikova, Z.A., Antipin, M.Y., Ogibin, Y.N., Nikishin, G., 2007. Deoxyholic acid-derivatized tetraoxane antimalarials and antiproliferatives. J. Med. Chem. 50, 5118–5127.

Thannickal, V.J., Fanburg, B.L., 2000. Reactive oxygen species in cell signaling. Am. J. Physiol. Lung Cell Mol. Physiol. 279, L1005–L1028.

Tokuyasu, T., Masuyama, A., Nojima, K., McCullough, J., Kim, H.-S., Wataya, Y., 2001. Yingzhaosu A analogues: synthesis by the ozonolysis of unsaturated hydroperoxides, structural analysis and determination of anti-malarial activity. Tetrahedron 57, 5979–5989.

Trape, J.F., 2001. The public health impact of chloroquine resistance in Africa. Am. J. Trop. Med. Hyg. 64, 12–17.

Tsuchiya, K., Hamada, Y., Masuyama, A., Nojima, M., McCullough, K.J., Kim, H.-S., Shibata, Y., Wataya, Y., 1999. Synthesis, crystal structure and anti-malarial activity of novel spiro-1, 2, 4, 5-tetraoxacycloalkanes. Tetrahedron Lett. 40, 4077–4080.

Warhurst, D.C., 1999. Drug resistance in *Plasmodium falciparum* malaria. Infection 27, S55–S58.

Winstanley, P.A., Ward, S.A., Snow, R.W., 2004. Clinical status and implications of antimalarial drug resistance. Microbes Infect. 4, 157–164.

Cancer Chemother Pharmacol (2009) 63:837–850
DOI 10.1007/s00280-008-0810-y

ORIGINAL ARTICLE

Role of RNase L in apoptosis induced by 1-(3-*C*-ethynyl-β-D-*ribo*-pentofuranosyl)cytosine

Tomoharu Naito · Tatsushi Yokogawa · Satoshi Takatori · Kazato Goda · Akiko Hiramoto · Akira Sato · Yukio Kitade · Takuma Sasaki · Akira Matsuda · Masakazu Fukushima · Yusuke Wataya · Hye-Sook Kim

Received: 30 April 2008 / Accepted: 18 July 2008 / Published online: 31 July 2008

Abstract
Purpose 1-(3-*C*-Ethynyl-β-D-*ribo*-pentofuranosyl)cytosine (ECyd), a ribonucleoside analog, has a potent cytotoxic activity against cancer cells. The present studies have been performed to elucidate the overall mechanisms of ECyd-induced apoptotic cell death.
Methods Cultured cells of mouse mammary carcinoma FM3A and human fibrosarcoma HT 1080 lines were used. The efficacy of RNA synthesis inhibition by ECyd was assessed by kinetic analysis using nuclei isolated from FM3A cells. RNA status in ECyd-treated cells was investigated by Northern blots, and the cleavage sites of RNA were identified by rapid amplification of 5′ cDNA ends (5′-RACE). The effect of protein functions on the ECyd-induced apoptotic pathway was analyzed by siRNA and immunohistochemical techniques. Apoptotic cells were detected by TdT-mediated dUTP-biotin Nick End Labeling (TUNEL) assay.
Results ECyd induces inhibition of RNA synthesis in vitro and in vivo, which appears to be a major cause for the apoptosis. It is known that ECyd is converted inside the cell into its 5′-triphosphate (ECTP). We have now found in test-tube experiments that ECTP strongly inhibits the activity of RNA polymerase I by competing with CTP. In the absence of robust RNA synthesis, the cellular RNAs would be destined to break down. RNase L was found to be playing a role in the breakdown: thus, the 28S rRNA-fragmentation pattern observed for the ECyd-treated cells was very similar to that observable in an in vitro treatment of the 28S ribosomes with RNase L. Association of RNase L with the cytotoxic action of ECyd was confirmed by use of the siRNA-mediated suppression of the cellular RNase L. Thus, the cells in which the RNase L was knocked-down were highly resistant to the cytotoxic action of ECyd. Further events, downstream of the RNase L action that can lead to the eventual apoptosis, would conceivably involve the phosphorylation of c-jun N-terminal kinase and subsequent decrease in mitochondrial membrane-potential. Evidence to support this flow of events was obtained by siRNA-experiments.
Conclusion The results from this study demonstrated that RNase L is activated after the inhibition of RNA polymerase, and induces mitochondria-dependent apoptotic pathway. We propose this new role for RNase L in the apoptotic mechanism. These findings may open up the possibility of finding new targets for anticancer agents.

Keywords ECyd · RNase L · JNK · Apoptosis · RNA synthesis · 28S rRNA fragmentation

Tomoharu Naito and Tatsushi Yokogawa have contributed equally to the main findings of the paper.

T. Naito · T. Yokogawa · S. Takatori · K. Goda · A. Hiramoto · A. Sato · M. Fukushima · Y. Wataya · H.-S. Kim (✉)
Faculty of Pharmaceutical Sciences,
Okayama University, 1-1-1 Tsushimanaka,
Okayama 700-8530, Japan
e-mail: hskim@cc.okayama-u.ac.jp

Y. Kitade
Department of Biomolecular Science,
Faculty of Engineering, Gifu University,
1-1 Yanagido, Gifu 501-1193, Japan

T. Sasaki
Cancer Research Institute, Kanazawa University,
13-1 Takara-machi, Kanazawa 920-0934, Japan

A. Matsuda
Graduate School of Pharmaceutical Sciences,
Hokkaido University, Kita-12 Nishi-6,
Kita-ku, Sapporo 060-0812, Japan

Introduction

Many anticancer agents are DNA synthesis-inhibitors, targeting at the rapidly proliferating tumor cells. However, their effects on solid tumors are often unsatisfactory. Between solid tumor- and normal-cells, the growth rates are not greatly different. In solid tumors, the proportion of cell number at the S phase is smaller than that of the rapidly proliferating tumor cells, and the cells in solid tumors are heterogeneous in the sense that individual cells activate various phases of cell cycle. For this reason, we considered the need for the inhibition of RNA synthesis, which occurs throughout the cell cycle except in the M phase, to potentiate the anticancer effect against solid tumors.

1-(3-*C*-Ethynyl-β-D-*ribo*-pentofuranosyl)cytosine (ECyd), a nucleoside analog originally designed as a possible inhibitor of cellular RNA synthesis, has been shown to exhibit strong activities against carcinogenesis [1, 2]. In our earlier experiments using cultured cells, we have shown that the metabolic conversion of ECyd into its active form, 5′-triphosphate (ECTP) takes place readily in cancer cells, but only very slowly in normal cells [3, 4]. It was noted that cellular RNA synthesis was indeed strongly inhibited, presumably by the presence of the CTP analog, ECTP, within the cell, and this inhibition appeared to trigger the apoptotic cell death. Although apoptosis-like cell death is induced in the ECyd-treated cells, it is still not clear what activates the apoptotic signal after the RNA synthesis inhibition. Identification of such factors may lead to devices for improving the antitumorigenic efficacy of ECyd. We have now performed extensive studies for elucidating the overall picture of the ECyd-induced death of cancer cells, mouse mammary carcinoma FM3A and human fibrosarcoma HT 1080. As described below, the flow of events leading to the apoptosis was largely revealed; a process in which RNase L plays an important role.

Materials and methods

Materials

ECyd was synthesized as described previously [2]. Actinomycin D and ara-C were purchased from Sigma-Aldrich (St Louis, MO, USA). [8-^{3}H]GTP and [γ-^{32}P]ATP were obtained from Amersham Biosciences (Piscataway, NJ, USA). Oligonucleotides used in Northern blot hybridization and in RACE (Rapid Amplification of 5′ cDNA Ends) were obtained from Sawady Technology (Tokyo, Japan). RNase T_1, RNase A, lipofectin and lipofectamine 2000 were purchased from Invitrogen (Carlsbad, CA, USA). Human recombinant RNase L was prepared as described previously [5]. The 2-5A used was p5′(A2′p5′)$_2$A synthesized as reported [6]. The antibody to c-jun NH_2-terminal kinase (JNK) was from Cell Signaling Technology (Beverly, MA, USA), that to β-actin was from Sigma-Aldrich, and that to GAPDH was from Trevigen (Gaithersburg, MD, USA). Preparation of monoclonal antibody to human RNase L and synthesis of siRNA were done as previously reported [7]. A pair of RNase L-siRNA (siRNL) and control siRNA (siMis) were prepared as reported [7]. The sequences of these siRNAs were as follows: active siRNAs (siRNL) 5′-GCUGUUCAAAACGAAGAUGTT-3′ 3′-TTCGACA AGUUUUGCUUCUAC-5′; control siRNAs (siMis) 5′-GC UAUUCUAAAGGAAUAUGTT-3′ 3′-TTCGAUAAGA UUUCCUUAUAC-5′. The TT dinucleotide attached to each of these oligonucleotides at their 3′ overhang was a deoxythymidine dimer with a carbamate linkage that enhances the siRNA silencing activities.

Cell culture and drug treatments

The cultivation of cells, mouse mammary tumor FM3A (F28-7, Japanese Cancer Research Resources Bank, Tokyo, Japan) and human fibrosarcoma HT 1080 (American Type Culture Collection, Rockville, MD, USA), was performed as previously reported [3, 4]. In several experiments, it was difficult to use FM3A because the cells are suspension-cultured cell lines lacking adhesive characters. In such cases, we used adhesive type cells HT 1080. Cell viability was estimated by the trypan blue exclusion method using a hemocytometer. The 50% growth-inhibitory concentration of ECyd against FM3A and HT 1080 cells is 3×10^{-8} M and 1.3×10^{-8} M, respectively. For each cell line, drug treatments were performed at doses 100-fold, the 50% growth-inhibitory concentration.

Transfection

Transfections of 2-5A and siRNAs were done using lipofectin and lipofectamine 2000 according to the manufacturer's protocols.

Kinetic analysis of RNA synthesis with isolated nuclei

Nuclei from exponentially growing FM3A cells (1×10^8) were prepared and an RNA synthesis reaction was performed by the method of Marzluff and Huang [8]. The reaction mixtures contained 500 μM each of ATP and UTP, 50 μM [8-^{3}H]GTP, 6–18 μM CTP, and 0–40 nM ECTP, and nuclei at $2-5 \times 10^7$/mL. For kinetic analysis of the effect of ECTP on RNA polymerase, the initial incorporation rates of radioactivity into the acid-insoluble fraction were measured.

Immunohistochemistry

The histochemical study was performed on HT 1080 cells to observe the localization of fibrillarin in nucleolus and to explore the phosphorylation of JNK in ECyd-treated cells. After ECyd-treatment, HT 1080 cells were placed on cover glass plates. The cells were washed three times with PBS and fixed with 3% formaldehyde in PBS for 10 min. After fixation, the cells were washed twice with PBS, and were made permeable by treatment with 0.2% Triton X-100 in cold PBS for 5 min. The slides were then incubated with PBS containing 0.5% BSA as a blocking agent against non-specific surface adsorption of antibodies, for 30 min prior to treatment for 1 h with 2.5 μg/ml anti-fibrillarin antibody (Cytoskeleton, Denver, CO, USA). The same procedure was performed using 1 μg/ml anti- phosphorylated-JNK and anti-total-JNK antibodies (Cell Signaling Technology) for overnight at 4°C. The cells were then incubated with 5 μg/ml fluorescein-labeled goat anti-mouse IgG and 1 μg/ml 4′,6-diamidino-2-phenylindole dihydrochloride (DAPI) for 30 min. The cells were washed three times with PBS and covered with PermaFluor aqueous mounting medium (Invitrogen, Oregon, USA). Stained cells were observed with an Olympus BX60 microscope (Olympus, Tokyo, Japan) fitted with appropriate fluorescence filters.

Preparation of RNA and Northern blots

For the preparation of total RNA from FM3A and HT 1080 cells, QIAshredder and RNeasy kits were used (Qiagen, Hilden, Germany). RNA (2 μg/ml) was denatured in formaldehyde and then electrophoresed on a 1% agarose–formaldehyde gel. The RNA was then transferred to a Hybond-N^+ nylon membrane (Amersham, Piscataway, NJ, USA) and hybridized to ^{32}P-labeled DNA probes. The sequences of oligonucleotide probes are shown in Table 1.

Rapid amplification of 5′ cDNA ends

To identify 5′-terminal sequences of the 1.5 kb fragment formed from 28S rRNA on ECyd-treatment, 5′-RACE was performed with a kit for rapid amplification of cDNA ends (version 2.0, Invitrogen). The following oligonucleotides were used: 5′-TCAAGCTCAACAGGGTCT-3′ (antisense of nucleotides 3561–3578) for the first-strand cDNA synthesis and 5′-CGCTGGATAGTAGGTAGGGA-3′ (antisense of nucleotides 3495–3514) for the subsequent PCR. Amplified cDNA was sequenced by a sequencer (PRISM 310, ABI).

Preparation of ribosomal fractions

FM3A cells (1×10^8) were spun down, washed twice with ice-cold PBS, and resuspended in 1.5 volumes of 20 mM KCl, 5 mM Tris–HCl (pH 7.6), 1.25 mM Mg acetate, and 1.25% glycerol, and then homogenized with a Teflon-Potter homogenizer. The homogenates were centrifuged for 15 min at $16{,}000\times g$ to remove insoluble materials. Ribosomes were obtained by centrifuging cellular lysate (0.7 ml, corresponding to 5×10^7 cells) prepared as above through a cushion of 1.3 M sucrose, 50 mM Tris–HCl (pH 7.6), 2 mM $MgCl_2$, 50 mM KCl at $190{,}000\times g$ for 2.5 h at 4°C. The ribosomes were resuspended in 0.25 mM sucrose, 50 mM Tris–HCl (pH 7.6), 2 mM $MgCl_2$, and 50 mM KCl, and stored in aliquots at −80°C.

rRNA cleavage assay

RNase L (0.2 μg/ml) was pre-incubated in the presence of 120 nM 2-5A in 20 mM Tris–HCl (pH 7.5), 10 mM Mg acetate, 8 mM 2-mercaptoethanol, 90 mM KCl at 0°C for 30 min, prior to the addition of ribosomes (corresponding to 3 μg rRNA). The cleavage reactions were performed in a final volume of 20 μl with an incubation at 30°C. RNase A and RNase T_1 were individually incubated with ribosomes in 0.3 mM NaCl at 30°C for desired periods. These reaction mixtures were then diluted tenfold with 100 mM Tris–HCl (pH 8.0), 100 mM NaCl, 1 mM EDTA, and RNA was extracted with phenol, and the aqueous phase was re-extracted and the cleavage products were analyzed by a 2.2% agarose gel-electrophoresis.

Table 1 Northern hybridization with the specific probes for mouse and human 28S rRNA in ECyd-treated cells

	Probe sequence	Position in 28S rRNA	
		Mouse	Human
1.	5′-CCGTTACTGAGGGATCCTGGTTAGTTTCTTTTCCTCCGC-3′	52–91	52–91
2.	5′-AAAGGACGGGGGGTCTCCCCGG-3′	2,731–2,752	
3.	5′-GGGTTGGACCCGCCGCCCCGGAG-3′	2,876–2,898	
4.	5′-GAACACCGACGCGGAGGTTC-3′	3,167–3,186	
5.	5′-GCGGGCCTTCGCGATGCTTTGTT-3′	3,303–3,325	
6.	5′-ACCCAGAAGCAGGTCGTCTACGAATGGTTTAGCGCCAG-3′	4,610–4,648	4,610–4,648

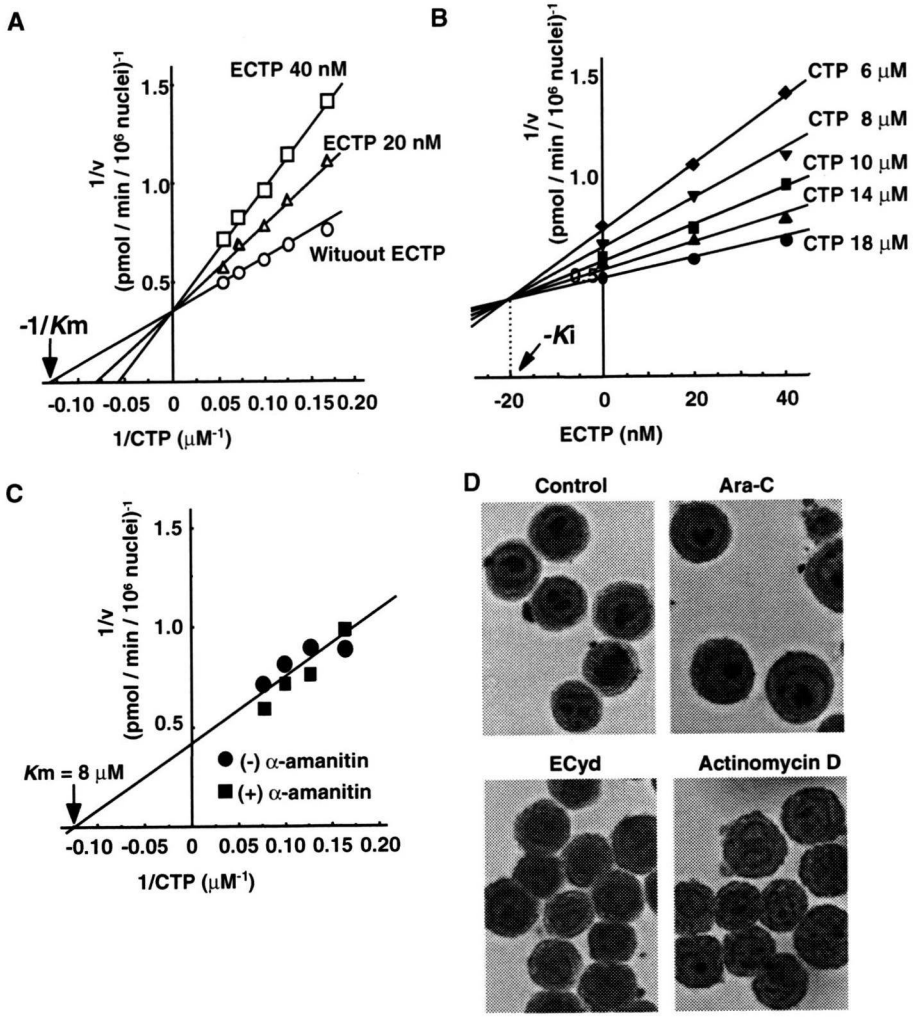

Fig. 1 Kinetic analysis of the effect of ECTP on RNA polymerase I in isolated nuclei. The K_m value for CTP and the K_i value for ECTP were determined by a Lineweaver-Burk plot (**a**) and a Dixon plot (**b**), respectively. **c** The effects of α-amanitin on RNA synthesis in isolated nuclei from FM3A cells. α-Amanitin was used at 100 μg/ml. *Points* means of triplicate analysis with ±SD of less than 5%. **d** The morphological changes in nucleoli were evaluated with Azure C staining in FM3A cells. FM3A cells were treated with either ECyd (3 μM), actinomycin D (0.21 μM) or ara-C (44 μM) for 4 h

Western blotting

HT 1080 cells were suspended in 20 mM HEPES (pH 7.5), 10 mM K acetate, 15 mM Mg acetate, 1 mM dithiothreitol, 1 mM phenylmethyl sulfonylfluoride, 10 μg/ml aprotinin, and 0.5% (v/v) Nonidet P-40, and homogenized with a tight-fitting glass Dounce homogenizer on ice. Insoluble materials were removed by centrifugation at 10,000×*g* (at 4°C for 10 min). Proteins in soluble fractions were separated on 7.5% polyacrylamide gels containing SDS and transferred to polyvinylidene difluoride membranes (Millipore, Bedford, MA, USA). For detection of phosphorylated JNK, HT 1080 cells were homogenized in Phosphosafe Extraction Buffer (Novagen, Madison, WI, USA). After cell lysis, the samples were centrifuged at 16,000×*g* for 5 min. Proteins (20 μg) were separated by 12.5% polyacrylamide gel-electrophoresis. Western blotting was done with individual antibodies. The secondary antibodies used were horseradish peroxidase-conjugated anti-mouse IgG antibody (Amersham). Immunoreactive bands were detected by enhanced chemiluminescence (Amersham) and subsequent exposure to X-ray film.

TUNEL assays

HT 1080 cells were plated onto glass coverslips precoated with poly-L-lysine. According to the TUNEL protocol (#TB235; Promega, Madison, WI, USA), cells were washed with PBS, fixed with 4% paraformaldehyde for 25 min, and rinsed three times with PBS. Cells were then permeabilized with 0.2% Triton X-100 in PBS, rinsed twice with PBS, and equilibrated with 100 μl of equilibration buffer at room temperature for 10 min. The DNA nick-labeling reaction was performed using 50 μl terminal deoxynucleotidyl transferase (TdT) incubation-buffer. The buffer contained 45 μl equilibration buffer, 5 μl nucleotide mix including fluorescein-12-dUTP (Promega, Madison, WI, USA) and 1 μl TdT for 60 min at 37°C. The reaction

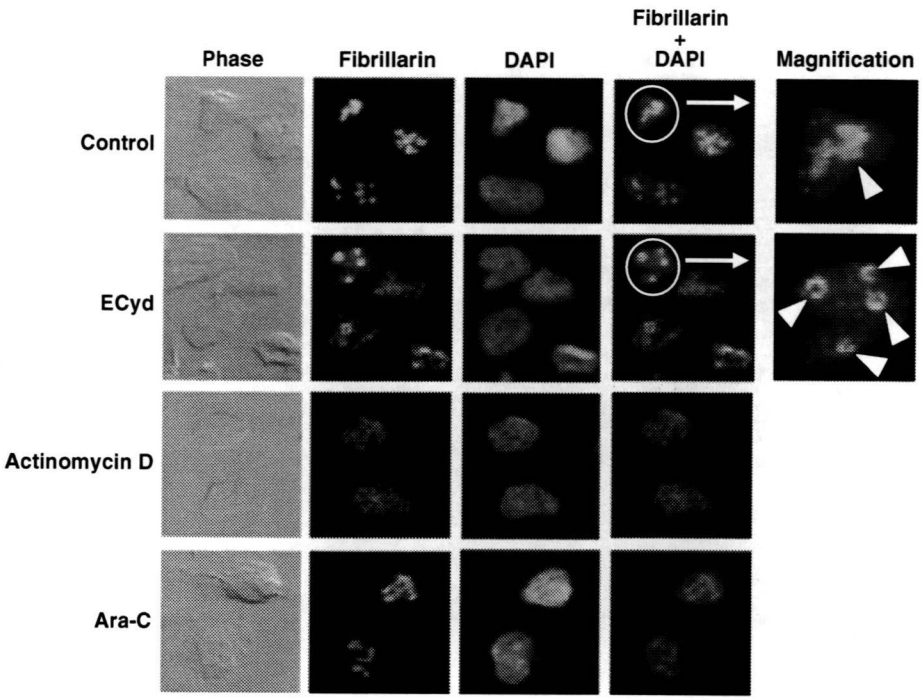

Fig. 2 Localization of fibrillarin in ECyd-treated cells. HT 1080 cells were treated with *ECyd* (1.3 μM), *actinomycin D* (25 μM) or *ara-C* (34 μ) for 4 h. Immunolocalization of *fibrillarin* (*green*) and nuclear morphology (*blue*) was visualized by confocal immunofluorescence microscopy. Nuclei were stained with *DAPI*

was then terminated by immersing the slides in 2× SSC for 15 min at room temperature. The samples were rinsed three times with PBS and mounted for analysis under a fluorescence microscope using a standard fluorescein filter, set to view through the microscope using standard fluorescein at 520 nm.

Radiolabelled RNase L substrate assay

HT 1080 cells were washed once with PBS, scraped into a minimal volume of ice-cold PBS and pelleted at 500×*g* for 5 min. Pellets were stored at −70°C until required. Pellets were then lysed in approximately twice the pellet volume of the cell lysis reagent (Sigma). After 15 min on ice, the lysate was centrifuged and the protein concentration was measured (Pierce, Rockford, IL, USA). A synthetic oligoribonucleotide $C_{11}UUC_7$ was end-labeled with [^{32}P]ATP using T4-polynucleotide kinase (Qiagen) for use as a probe. The labeled oligoribonucleotide was then purified using a spin column with twice washing with 10 mM Tris, and 1 mM EDTA (TE) and eluting with 50 μl of elution buffer. A 2.5 μg of protein in cell lysates was incubated with 2 μl of labeled probe in 20 μl of reaction mixture for 30 min at 30°C. Electrophoresis was performed on a 20% acrylamide/7 M urea/Tris–borate–EDTA (TBE) gel followed by autoradiography. Aliquots of each protein sample were subjected to Western blotting using probes for RNase L and GAPDH.

Detection of mitochondrial membrane potential

HT 1080 cells were stained with the cationic dye, 5,5′,6,6′-tetrachlorol-1′,3,3′-tetraethyl-benzimidazolylcarbocyanine iodide (JC-1; Molecular Probes) to determine the state of mitochondrial membrane potential. JC-1 is a potentiometric dye that exhibits a membrane potential-dependent loss. HT 1080 cells were incubated with RPMI1640 medium containing 10% serum and 1 μg/ml JC-1 at 37°C for 15 min. Following incubation, the cells were rinsed twice with PBS and images were obtained using a fluorescence microscope (Olympus).

Results

ECTP was a strong and competitive inhibitor of RNA polymerase I

Earlier, we found that in cells ECyd is phosphorylated to ECTP, resulting in the inhibition of RNA synthesis without changing the normal ribonucleoside triphosphate pool [3]. This finding indicated that RNA synthesis is inhibited at the RNA polymerization step. To determine the inhibitory mechanism of polymerization, we investigated the inhibition of RNA synthesis by ECTP using nuclei isolated from FM3A cells. The results obtained by a Lineweaver-Burk plot indicated that ECTP inhibits the synthesis in a competitive

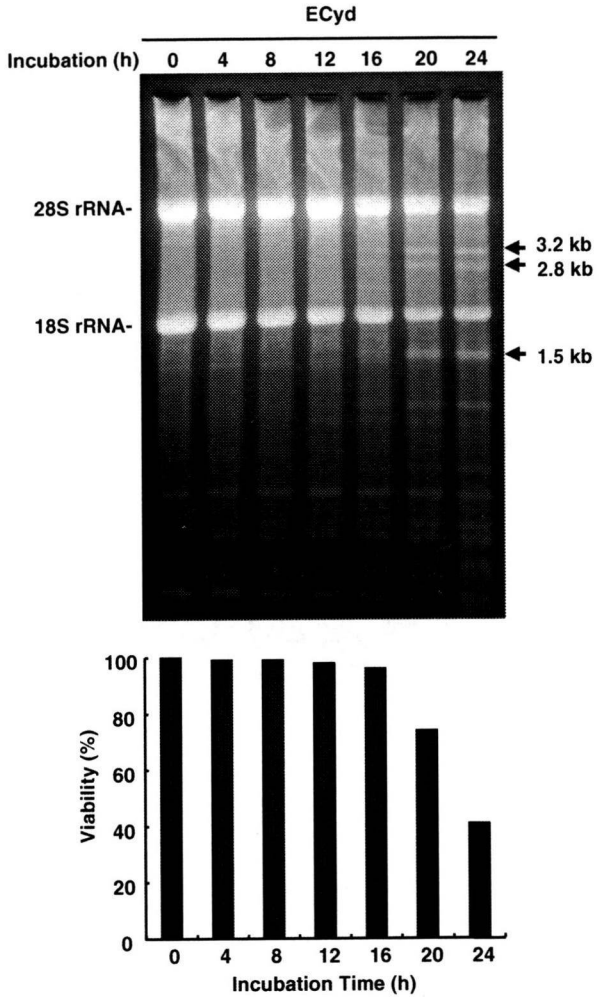

Fig. 3 28S rRNA fragmentation induced by ECyd-treatment. Total RNA was isolated at the indicated time from FM3A cells (3.7×10^5), that had been treated with ECyd (3 μM), and analyzed by 2.2% agarose gel electrophoresis. The cleavage products (3.2, 2.8 and 1.5 kb) are indicated by *arrows*. The cell viability was determined by the trypan blue staining, and the percentage of living cells was plotted on graph

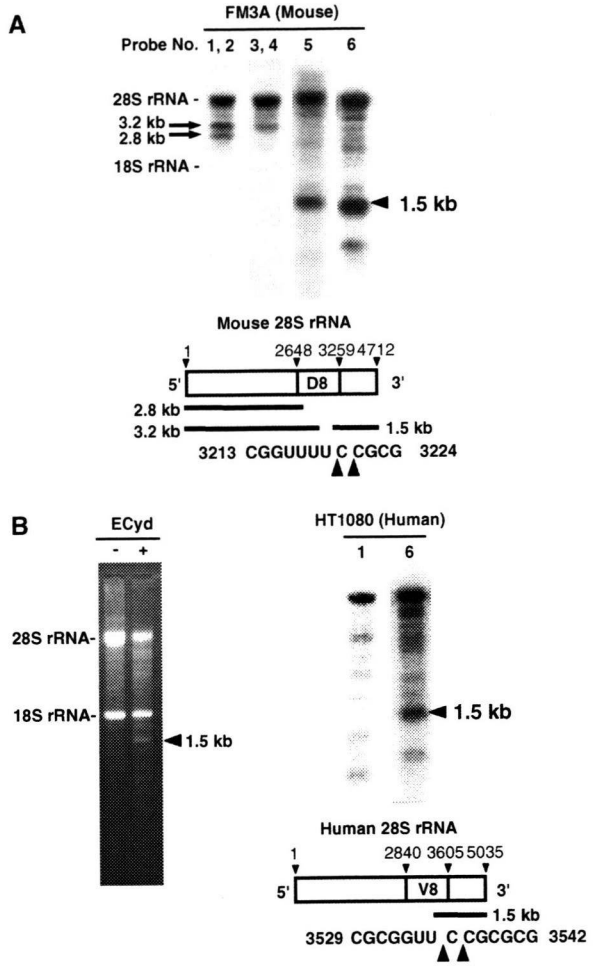

Fig. 4 Identification of rRNA fragments. **a** Northern blot analysis of fragmented rRNA. Total RNA was isolated from the FM3A cells that had been treated with ECyd (3 μM) for 24 h, electrophoresed, and subjected to Northern blotting with the labeled oligonucleotide probes as described in "Materials and methods". Fragments 3.2, 2.8 and 1.5 kb are highlighted by *arrows*. The 5′-terminal sequence of 1.5 kb was determined by 5′-RACE as described in Materials and methods". The cleavage sites are represented by *arrowheads*. nt, nucleotides. **b** *left column*: total RNA from HT 1080 cells that had been treated with ECyd (1.3 μM) for 32 h was separated by 2.2% agarose gel electrophoresis. The 1.5 kb fragment is indicated by an *arrow*. **b** *right column*: Northern blot analysis of 1.5 kb fragment, and identification of the cleavage site by 5′-RACE

manner (Fig. 1a). The apparent K_i value of ECTP for the RNA synthesis was 20 nM, as derived from the Dixon plot analysis (Fig. 1b). We used α-amanitin for positive controls in inhibiting RNA polymerase II and III. α-Amanitin at a concentration of 100 μg/ml was reported to be sufficient to inhibit both RNA polymerases II and III [9], and it showed in our hands little effect on the velocity of the RNA synthesis, may be indicating that the RNA synthesis in nuclei occurs mainly by RNA polymerase I (Fig. 1c). Nucleoli are the main intracellular location sites for RNA polymerase I, a key enzyme involved in the transcription process of pre-ribosomal RNA (pre-rRNA) during initial ribosome biogenesis. Following treatment of FM3A cells with ECyd, nucleolus shrinkage was observed within 4 h after the RNA synthesis was inhibited. These morphological changes in the nucleoli were also observed by actinomycin D, an inhibitor of RNA synthesis, but not by ara-C, an inhibitor of DNA synthesis (Fig. 1d).

ECyd induced characteristic nucleolar changes subsequent to RNA synthesis inhibition

Using human cancer cell line HT 1080, we observed the changes of nucleolus by detecting fibrillarin in ECyd-treated

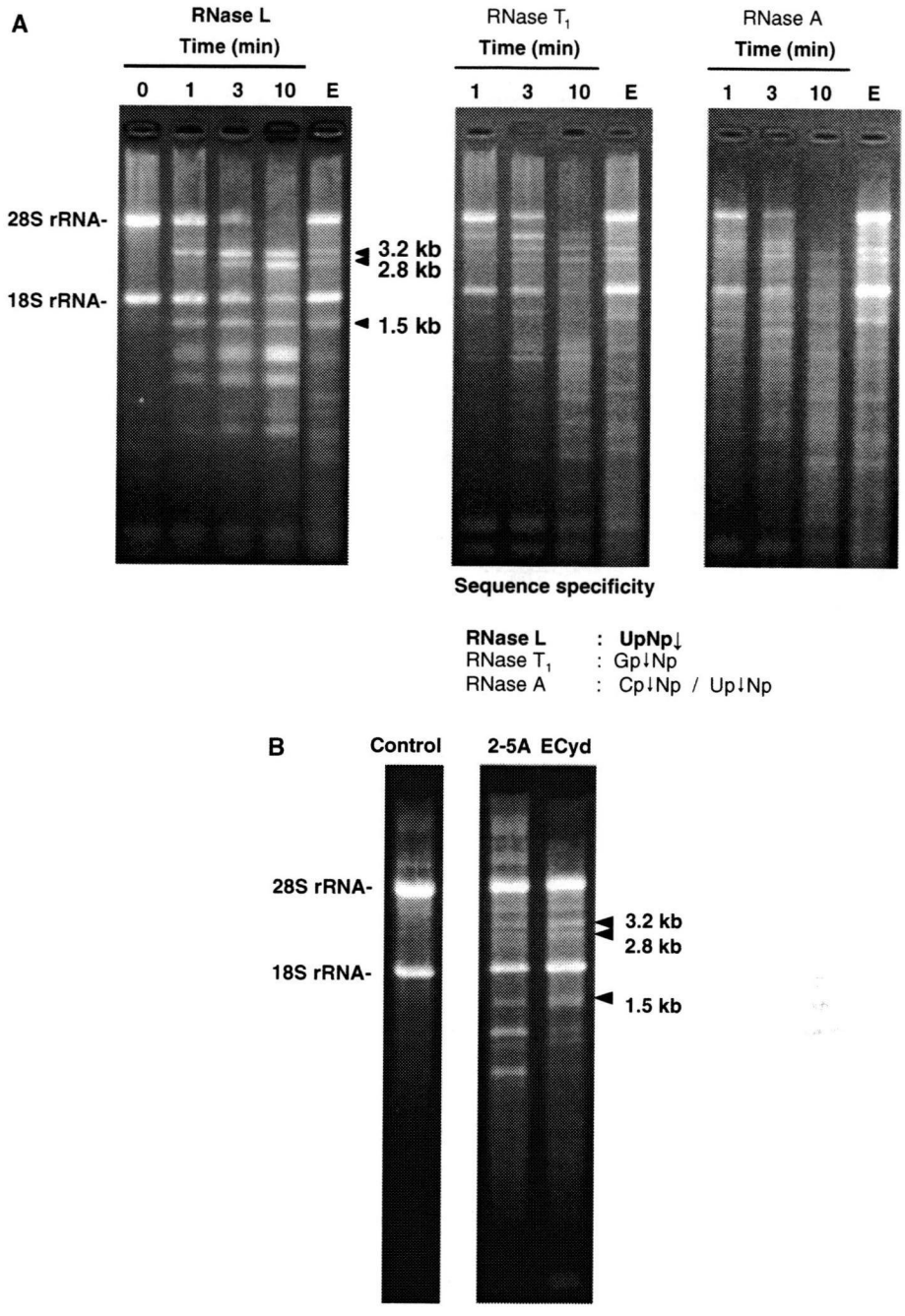

Fig. 5 The fragmentation pattern of rRNA induced by ECyd-treatment was identical to that cleaved by RNase L. *A*, Ribosomal fractions (corresponding to 3 μg RNA) prepared from FM3A cells were incubated with human RNase L (0.2 μg/ml) in the presence of 2-5A (120 nM). RNase A and RNase T_1 were incubated with ribosomes in 0.3 mM NaCl at 30°C for the indicated time. *E* ECyd-treatment induces 28S rRNA fragmentation pattern. The sequence recognized by RNase L, T1 and A are shown. **b** FM3A cells were treated with 2-5A (5 μM) in the presence of lipofectin (2 μg/ml) for 4 h according to the manufacturer's protocol (Invitrogen). The control shows cells treated with lipofectin only. The cleavage products were analyzed by 2.2% agarose gel electrophoresis

cells. Fibrillarin, a protein scatteringly located in the nucleoli, is directly involved in many post-transcriptional processes such as pre-rRNA processing, pre-rRNA methylation and ribosome assembly [10]. As shown in Fig. 2, control cells with no drug treatment showed bright clumpy nucleolar staining. Treatment with ECyd caused dislocation of fibrillarin within 4 h and formed ring-like structures, possibly involving remnant nucleoli (Fig. 2). Dispersion of fibrillarin was also induced by actinomycin D [11], but not by ara-C.

Considering that this nonhomogeneous distribution of fibrillarin was probably caused by the depletion of pre-rRNA, we monitored the amount of rRNA, a resultant product of pre-rRNA processing, in ECyd-treated FM3A cells. The amount of rRNA had decreased to 67% from the basal amount at 8 h after treatment with ECyd. Moreover, an

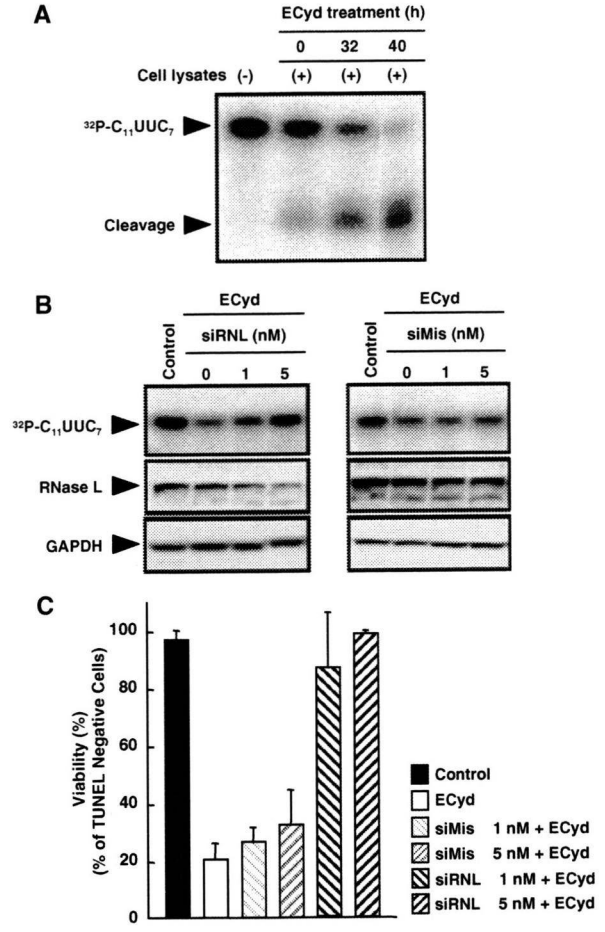

Fig. 6 RNase L activity assay demonstrating cleavage of a radiolabeled RNase L-specific substrate (5′ ^{32}P-$C_{11}UUC_7$). **a** A single-stranded RNA probe ($C_{11}UUC_7$) was end-labeled with [^{32}P]ATP and incubated with lysates prepared from ECyd-treated HT 1080 cells for indicated times. **b** RNA probe was incubated with lysates from ECyd-treated cells with siRNL or siMis. *siRNL* siRNA against RNase L. *siMis* a 4-bp mismatch introduced in RNase L siRNA. After incubation, the reaction mixtures were run on an acrylamide gel followed by autoradiography and Western blotting using antibody for RNase L and GAPDH. **c** Apoptotic cells were measured by TUNEL assays in triplicate, and ±SD were calculated

extensive fragmentation of rRNA was observed at 16 h of the treatment, accompanying a decrease in viability (Fig. 3).

rRNA fragmentation occurred in the D8 domain of 28S rRNA after treatment of cells with ECyd

In ECyd-treated FM3A cells, characteristic 3.2, 2.8, and 1.5 kb bands of RNA were formed. This was accompanied by decreases in the amounts of 28S rRNA (Fig. 3). To verify whether these fragments were derived from 28S rRNA, Northern blot analysis was performed with specific probes for various parts of 28S rRNA. Both 3.2 and 2.8 kb bands hybridized with a probe for the 5′-terminal of 28S rRNA, while a 1.5 kb band hybridized with a probe for the 3′-terminal of 28S rRNA (Fig. 4a). In contrast, the probe for 18S rRNA failed to detect any corresponding bands (data not shown). A 3.2 kb band was detected with a probe No. 4 but not with No. 5. The 2.8 kb band was detected with probe No. 2 but not with No. 3. These data indicate that 3.2 and 2.8 kb bands were the products of 28S rRNA cleavage and those sites were at somewhere from 3186 to 3303, and from 2752 to 2876, respectively (Table 1). To determine the cleavage site in mouse 28S rRNA, the 1.5 kb fragment was isolated, followed by 5′-RACE to analyze its 5′-terminal sequence. As a result, the 5′-end base of the 1.5 kb fragment was found to be nucleotide 3219 U or 3220 C (Fig. 4a). These data confirmed that the fragmented bands originated from D8 domain [12].

Similar RNA fragmentation was observed for the human cell line HT 1080 as well. Thus, as Fig. 4b shows, ECyd-treated HT 1080 gave the 1.5-kb RNA fragment in the Northern blot analysis, and the cleavage site was identified as UpNp (Np being 3535 Up or 3536 Cp). This observation suggests that the ECyd-induced apoptosis is associated with this specific rRNA-fragmentation in a ubiquitous fashion.

The ECyd-induced cleavage pattern of rRNA was similar to that induced by RNase L, and their cleavage sites were identical.

It was reported that the D8 domain of rRNA is placed on the surface of the 60S subunit, and that it could be cleaved by some RNases [12–14]. To examine whether or not 28S rRNA is cleaved by RNase L in FM3A cells treated with ECyd, the isolated ribosomal fraction from FM3A cells was subjected to hydrolysis by human recombinant RNase L. Remarkably, the RNase L-cleaved fragmentation pattern of rRNA was similar to that of ECyd-induced one (Fig. 5a). On the other hand, two other enzymes with different sequence preferences, RNase T_1 and RNase A, showed different cleavage patterns (Fig. 5a). To activate intrinsic RNase L, 2-5A transfected FM3A cells can be used. The 28S rRNA fragments of 3.2, 2.8, and 1.5 kb were indeed formed by the 2-5A treatment (Fig. 5b). In addition, the 5′-ends of the 1.5 kb fragments derived from cleavage either by recombinant RNase L or by the 2-5A transfection were identical, as determined by the RACE-assay (data not shown).

RNase L was activated, and it caused apoptosis in ECyd treated cells

To verify the RNase L activity, we measured the cleavage pattern of radiolabeled oligonucleotide, $C_{11}UUC_7$ containing a consensus RNase L cleavage site (UpNp). In fact, the oligonucleotide was cleaved on incubation with ECyd-

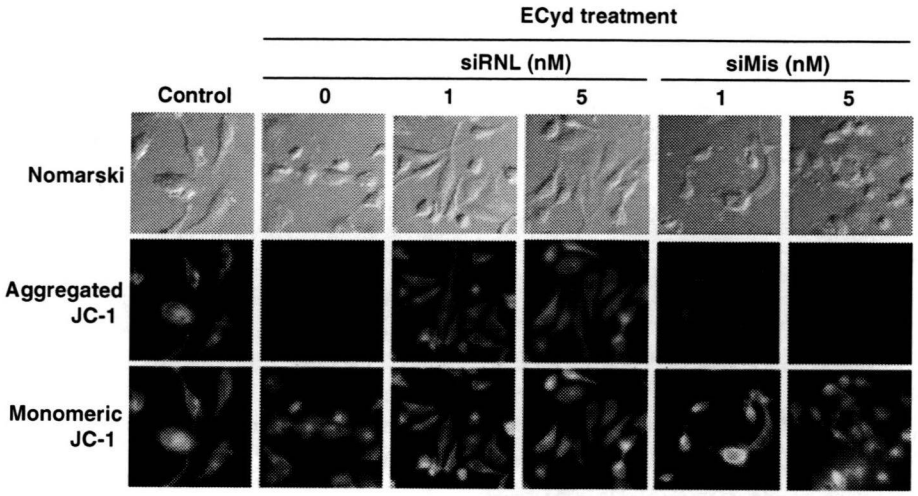

Fig. 7 The effect of RNase L-knockdown for mitochondrial membrane potential in the ECyd-treatment. HT 1080 cells were transfected with siRNL or siMis (1 or 5 nM) for 24 h prior to ECyd-treatment for 32 h (1.3 μM) and then JC-1 (molecular probes) treatment for 15 min at 37°C. *siRNL* siRNA against RNase L. *siMis* a 4-bp mismatch introduced in RNase L siRNA. In the picture "*Aggregated JC-1*", incorporation of JC-1 aggregates with *red fluorescence* into polarized mitochondria (normal mitochondria) can be seen. In contrast, in the picture "*Monomeric JC-1*", JC-1 monomers with *green fluorescence* binding to the membrane of both normal and damaged mitochondria are presented. Fluorescence microscopy analysis was performed using appropriate filters for the red fluorescence ($\lambda_{excitation}$: 546 ± 12 nm band pass filter, $\lambda_{detection}$: >590 nm long-pass filter) and the green fluorescence ($\lambda_{excitation}$: 450–490 nm band pass filter, $\lambda_{detection}$: >515 nm long-pass filter). The set of data in a given column were obtained from image-photos taken with a fixed exposure time

treated HT 1080 cell lysates in a time-dependent manner (Fig. 6a). In addition, both, the degradation of the whole oligonucleotide and the RNase L protein-expression were suppressed by treatment with an externally added siRNA against RNase L in HT 1080 cells (Fig. 6b left column). In contrast, siRNA with a 4-base mismatch sequence had no effect either for the cleavage activity or for the RNase L protein-expression (Fig. 6b right column). Also, we confirmed that the level of whole oligonucleotide was decreased on incubation with a recombinant RNase L activated by 2-5A (data not shown). As might be expected, in the RNase L-knockdown HT 1080 cells, the ECyd-induced apoptosis was suppressed (Fig. 6c). On the other hand, mismatch siRNA-treatment did not influence ECyd-induced apoptosis (Fig. 6c). In another cell line, DLD-1, a human colon cancer cell, RNase L-knockdown again suppressed ECyd-induced apoptosis (data not shown). This observation suggests that these events may be a general phenomenon for various cells.

RNase L-mediated apoptosis was dependent on mitochondrial membrane potential

A treatment of HT 1080 cells with ECyd resulted in a disappearance of red fluorescence of aggregated JC-1, indicative of dissipation of mitochondrial membrane potential (Fig. 7 middle panel). Also, the morphology of mitochondria, as detected by green fluorescence from monomeric JC-1, was disrupted in ECyd-only treated cells (Fig. 7 lower panel). On the other hand, in RNase L-knockdown HT 1080 cells, both, the levels of red fluorescence due to aggregated JC-1 and green fluorescence of JC-1 on the mitochondrial membrane were similar to those of control cells (no ECyd, no siRNA). In a mismatched siRNA-treatment, the level of red fluorescence from aggregated JC-1 was decreased, and the mitochondria showed abnormal morphology.

The JNK phosphorylation was dependent on RNase L, and led the cell to apoptosis

Figure 8a shows the level of phosphorylated JNK in ECyd-treated HT 1080 cells. The level of phosphorylated JNK increased to its maximum at 24 h of ECyd-treatment (Fig. 8a). It was notable that total JNK level (phosphorylated plus unphosphorylated) did not show any changes. When we administered anthrapyrazolone SP600125, an inhibitor of JNK action, to HT 1080 cells prior to ECyd-treatment, the apoptosis was suppressed with SP600125, in a dose dependent manner (Fig. 8b, c).

In order to analyze the effect of RNase L on the phosphorylation of JNK in HT 1080 cells, siRNA for RNase L was used to knockdown the RNase L protein expression. The level of phosphorylated JNK was decreased in the knocked-down cells, whereas the JNK-phosphorylation was maintained high in both the ECyd-only and ECyd-plus-mismatching siRNA treatments (Fig. 9). On the other hand, the fluorescence levels, that represent total JNK, were the same in all of these treatments.

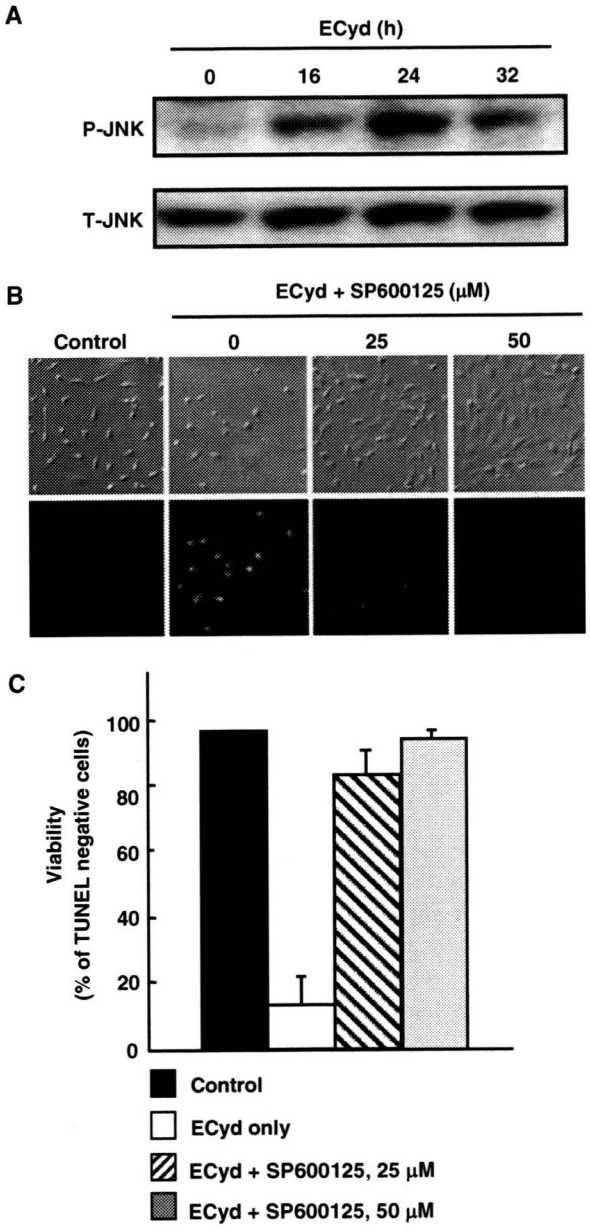

Fig. 8 The effect of JNK for ECyd-induced apoptosis. HT 1080 cells were treated with ECyd for 32 h in the absence or presence of Sp600125 (25 or 50 μM). **a** Western blots probed with antibodies to phosphorylated *JNK* (*P-JNK*) and total *JNK* (*T-JNK*) was performed at designated times of ECyd-treatment. **b** Changes in cellular morphologies. Green fluorescence represents apoptotic cells as a result of the TUNEL assay. **c** TUNEL-positive apoptotic cells were counted, and the percentage of apoptotic cells was plotted on a graph. Values are mean ± SD of triplicate samples at the indicated times

Figure 10 shows the change of mitochondrial membrane potential by treatment with JNK inhibitor, SP600125 in HT 1080 cells. As shown in the Figure, the mitochondrial membrane potential was resumed by the use of JNK inhibitor (Fig. 10 middle and lower panels). In contrast, ECyd-only treatment resulted in a null mitochondrial membrane potential.

Discussion

In this work, we show that ECyd induces nucleolar alterations and 28S rRNA fragmentation following the inhibition of RNA synthesis (Figs. 1, 2, 3). Actinomycin D, a known RNA synthesis inhibitor, also induces the change of nucleolar morphology. The interesting possibility that actinomycin D may induce similar RNA fragmentation in the cells is currently being explored. It should be noted that α-amanitin, an inhibitor to RNA polymerase-II and -III but not to RNA polymerase I [9], did not influence the velocity of RNA synthesis (Fig. 1c). These results suggest that ECyd induces inhibition of RNA polymerase I-activity. These disruptions in RNA status might represent a trigger mechanism for the apoptotic signaling pathway. Our results suggest that RNase L plays an important role for 28S rRNA fragmentation and for apoptosis induced by ECyd-treatment (Figs. 4, 5, 6). We show that RNase L mediates the apoptosis and the loss of mitochondrial membrane potential induced by ECyd treatment (Fig. 7). These suggest that the inhibition of RNA synthesis leads to mitochondria-dependent apoptosis, and that RNase L is required for this apoptosis. RNase L is a unique enzyme requiring $p(A2'p)_nA$ (2-5A), an unusual oligoadenylates with 2′–5′ phosphodiester linkages. 2-5A is produced from ATP by a family of 2′–5′ oligoadenylate synthetases (OAS) and binds to monomeric inactive RNase L to form a homodimeric active enzyme [15]. Previously, it was reported that the role of RNase L was to eliminate RNA-viruses in infected cells and to regulate the cell cycle, cell growth, and RNA metabolism with its endonucleolytic activity [16]. Our present study suggests that RNase L can potentiate the cellular suicidal pathway.

The inhibition of RNA synthesis has been shown by Morten et al. [17] to induce a morphological change in the nucleolus together with an alteration of nucleolar protein localization, prior to eventual apoptosis. Furthermore, RNA polymerase I is known to localize in the nucleolus where it transcribes rDNA to generate precursor transcripts of mature rRNA species. ECyd-treatment induced a morphological change of nucleoli in the nucleolus (Fig. 2), a phenomenon with which we hypothesize that the activity of RNA polymerase I might be inhibited in ECyd-treated cells. Our data also demonstrated that the events after the inhibition of RNA synthesis proceed via 2-5A/RNase L-activated pathway. Thus, RNase L is activated after nucleolar changes as a result of RNA synthesis inhibition (Fig. 6). Therefore, the RNase L-activating factor(s) may be produced under conditions of transcriptional inhibition. OAS requires ATP to produce the 2-5A, thereby RNase L is

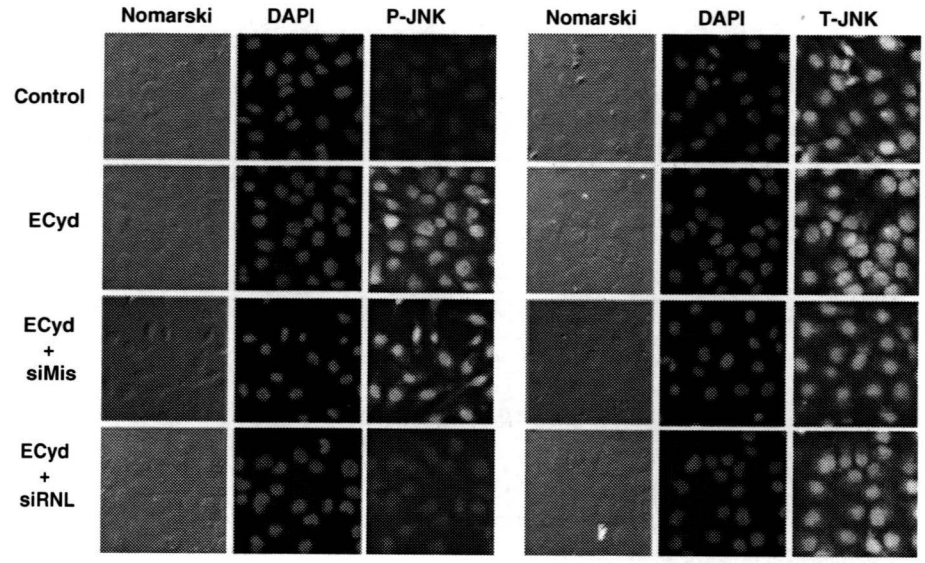

Fig. 9 The phosphorylation of JNK by RNase L. HT 1080 cells were transfected with siRNL and siMis 24 h prior to ECyd-treatment for 24 h. *siRNL* siRNA against RNase L. *siMis* a 4-bp mismatch introduced in RNase L siRNA. Phosphorylated JNK (*P-JNK*) and total JNK (*T-JNK*) were detected by immunofluorescence (IF) with specific antibody (Cell Signaling Technology). Nuclei were stained with *DAPI*. *Green fluorescence* represents IF: *P-JNK* and *T-JNK*. Control indicates lipofectamine-only treated cells. The set of data in a given column were obtained from image-photos taken with a fixed exposure time

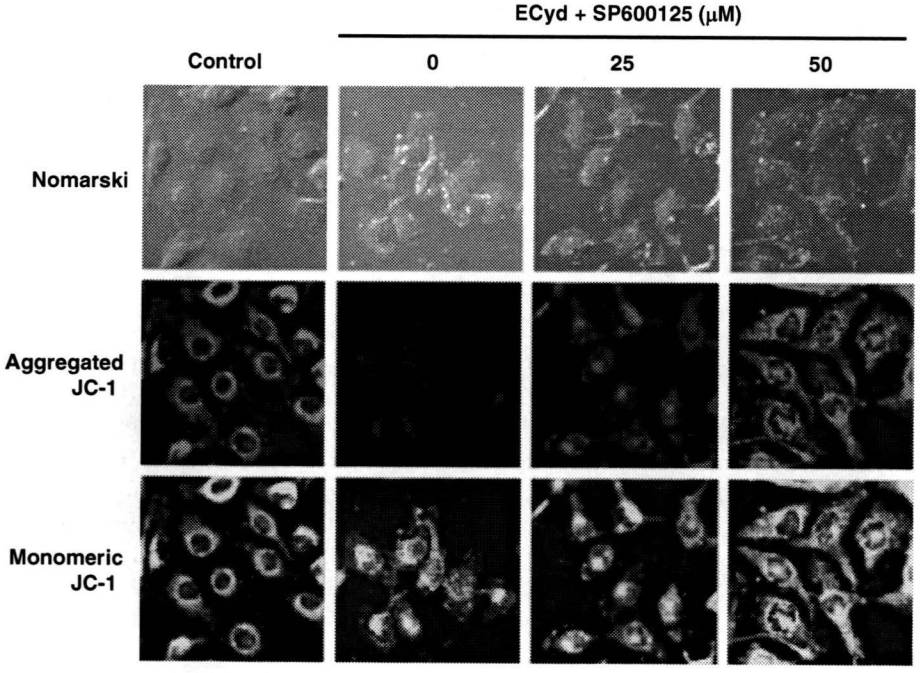

Fig. 10 The change of mitochondrial membarane potential by JNK phosphorylation. HT 1080 cells were treated with ECyd for 32 h in the absence or presence of JNK inhibitor Sp600125 (25 or 50 μM) and then were treated with JC-1 (Molecular Probes) for 15 min at 37°C. Mitochondrial depolarization was detected by using JC-1. In the picture "*Aggregated JC-1*", incorporation of JC-1 aggregates with *red fluorescence* into polarized mitochondria (normal mitochondria) can be seen. In contrast, in the picture "*Monomeric JC-1*", JC-1 monomers with *green fluorescence* bind to the membrane of both normal and damaged mitochondria are shown. Fluorescence microscopy analysis was performed using appropriate filters for the red fluorescence ($\lambda_{excitation}$: 546 ± 12 nm band pass filter, $\lambda_{detection}$: >590 nm long-pass filter) and the green fluorescence ($\lambda_{excitation}$: 450–490 nm band pass filter, $\lambda_{detection}$: >515 nm long- pass filter). The set of data in a given column were obtained from image-photos taken with a fixed exposure time

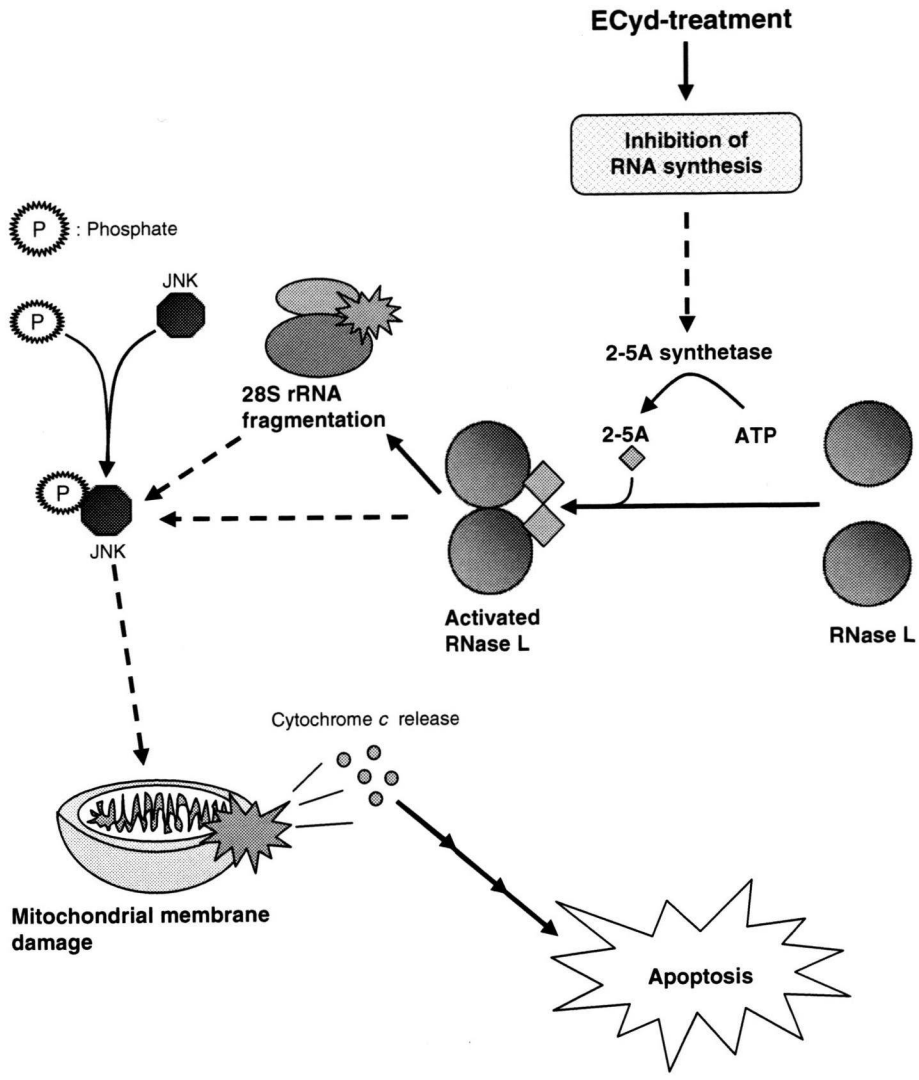

Fig. 11 Scheme of apoptotic signal pathway mediated by RNase L in ECyd-treated cells

activated. We have also reported that the intracellular concentration of ATP increased as a consequence of transcriptional inhibition in ECyd-treated FM3A cells [1]. Such ATP-rich environment would promote the OAS-mediated production of 2-5A. It was reported that OAS can be activated by RNA aptamers as well, in addition to activation by dsRNA [18]. Another report suggested that RNase L activation is associated with removal of abnormal cellular RNAs [19]. Thus, immature RNAs may possibly be produced in our experimental settings; thereby RNase L activation might become necessary to remove such abnormal RNAs in the cells. Although it is reported that a type of disruption of nucleolus structure can induce apoptosis, mechanisms involved in it is unknown [20].

It has been documented that activation of RNase L leads to activation of c-Jun N-terminal kinase (JNK), followed by mitochondrial release of cytochrome *c* and subsequent caspase-dependent apoptosis [21–23]. In our study, RNase L was activated and mitochondrial membrane potential was decreased in ECyd-treated cells. Therefore, it is expected that JNK phosphorylation may occur in the RNase L-dependent apoptotic signal pathway induced by ECyd. We investigated the phosphorylation of JNK in ECyd-treated HT 1080 cells. Indeed, JNK was found to be phosphorylated in these cells, and, moreover, a JNK inhibitor, SP600125, suppressed the apoptosis (Fig. 8). These data indicate that the ECyd-induced apoptosis is regulated by JNK signaling. The results shown in Figs. 9 and 10 support the notion that RNase L induces apoptosis through the phosphorylation of JNK. Thus, the apoptotic pathway may be summarily drawn as shown in Fig. 11. In addition, we have obtained data that suggest some aspects of downstream events: i.e., caspases -9 and -3 seem to be activated, subsequent to a release of cytochrome c from mitochondria,